INL/EXT-13-30203
Revision 0

Light Water Reactor Sustainability Program

Support and Modeling for the Boiling Water Reactor Station Black Out Case Study Using RELAP and RAVEN

September 2013

DOE Office of Nuclear Energy

INL/EXT-13-30203
Revision 0

Light Water Reactor Sustainability Program

Risk Informed Safety Margin Characterization (RISMC) BWR Station Blackout Demonstration Case Study

Diego Mandelli, Curtis Smith, Thomas Riley, John Schroeder, Cristian Rabiti, Andrea Alfonsi, Joe Nielsen
(Idaho National Laboratory)

Dan Maljovec, Bei Wang, Valerio Pascucci
(University of Utah)

September 2013

Idaho National Laboratory
Idaho Falls, Idaho 83415

http://www.inl.gov/lwrs

Prepared for the
U.S. Department of Energy
Office of Nuclear Energy
Under DOE Idaho Operations Office
Contract DE-AC07-05ID14517

EXECUTIVE SUMMARY

The existing fleet of nuclear power plants is in the process of extending its lifetime and increasing the power generated from these plants via power uprates. In order to evaluate the impact of these two factors on the safety of the plant, the Risk Informed Safety Margin Characterization (RISMC) project aims to provide insight to decision makers through a series of simulations of the plant dynamics for different initial conditions (e.g., probabilistic analysis and uncertainty quantification). This report focuses, in particular, on the impact of power uprate on the safety margin of a boiling water reactor. The case study considered is a loss of off-site power followed by the possible loss of all diesel generators, i.e., a station black-out (SBO) event. Analysis is performed by using a combination of thermo-hydraulic codes and a stochastic analysis tool currently under development at the Idaho National Laboratory, i.e. RAVEN.

Starting from an understanding of possible SBO accident sequences for a typical boiling water reactor, we built the input file for the mechanistic thermal-hydraulics code that models system dynamics under SBO conditions. We also interfaced RAVEN with these codes so that it would be possible to run multiple RELAP simulation runs by changing specific portions of the input files. We both employed classical statistical tools, i.e. Monte-Carlo, and more advanced machine learning based algorithms to perform uncertainty quantification in order to quantify changes in system performance and limitations as a consequence of power uprate. We also employed advanced data analysis and visualization tools that helped us to correlate simulation outcomes such as maximum core temperature with a set of input uncertain parameters.

Results obtained give a detailed investigation of the issues associated with a plant power uprate including the effects of SBO accident scenarios. We were able to quantify how the timing of specific events was impacted by a higher nominal reactor core power. Such safety insights can provide useful information to the decision makers to perform risk-informed margins management.

CONTENTS

FIGURES

TABLES

ACRONYMS

AC	Alternating Current
ADS	Automatic Depressurization System
BWR	Boiling Water Reactor
CCW	Component Cooling Water
CDF	core damage frequency
CST	Condensate Storage tank
DC	Direct Current
DOE	Department of Energy
DG	Diesel generator
DW	Drywell
EOP	Emergency Operating Procedures
HPCI	High Pressure Core Injection
HCTL	Heat Capacity Temperature Limits
INL	Idaho National Laboratory
LOCA	Loss of Coolant Accident
LOOP	Loss of offsite power
LOOPGR	Loss of Offsite Power Grid Related
LPCI	Low Pressure Core Injection
LWR	Light water reactor
LWRS	Light water reactor sustainability
MOOSE	Multi-physics Object-Oriented Simulation Environment
MSIV	Main Steam Isolation Valve
NPP	Nuclear power plant
PRA	Probabilistic risk assessment

PSP	Pressure Suppression Pool (also indicated as wetwell or torus)
PWR	Pressurized Water Reactor
PDF	Probability Distribution Function
R&D	Research and development
RCIC	Reactor Core Isolation Cooling
RHR	Residual Heat Removal
RISMC	Risk Informed Safety Margin Characterization
RIMM	Risk Informed Margin Management
RPV	Reactor Pressure Vessel
SPAR	Standardized Plant Analysis Risk
SRV	Safety Relief Valve
SVM	Support Vector Machine
SW	Service Water
T-H	Thermal-hydraulics

Risk Informed Safety Margin Characterization (RISMC)

1. THE RISMC APPROACH

In the RISMC [1] approach, what we want to understand is not just the frequency of an event like core damage, but how close we are (or not) to key safety-related events and how might we increase our safety margin through proper application of RIMM (Risk Informed Margin Management). In general terms, a "margin" is usually characterized in one of two ways:

- A deterministic margin, typically defined by the ratio (or, alternatively, the difference) of a capacity (i.e., strength) over the load.
- A probabilistic margin, defined by the probability that the load exceeds the capacity.

A probabilistic safety margin is a numerical value quantifying the probability that a safety metric (e.g., for an important process observable such as clad temperature) is exceeded under accident scenario conditions.

The RISMC Pathway uses the probabilistic margin approach to quantify impacts to reliability and safety. As part of the quantification, we use both probabilistic (via risk simulation) and mechanistic (via physics models) approaches, as represented in Figure 1-1. Probabilistic analysis is represented by the risk analysis while mechanistic analysis is represented by the plant physics calculations. Safety margin and uncertainty quantification rely on plant physics (e.g., T-H and reactor kinetics) coupled with probabilistic risk simulation. The coupling takes place through the interchange of physical parameters (e.g., pressures and temperatures) and operational or accident scenarios.

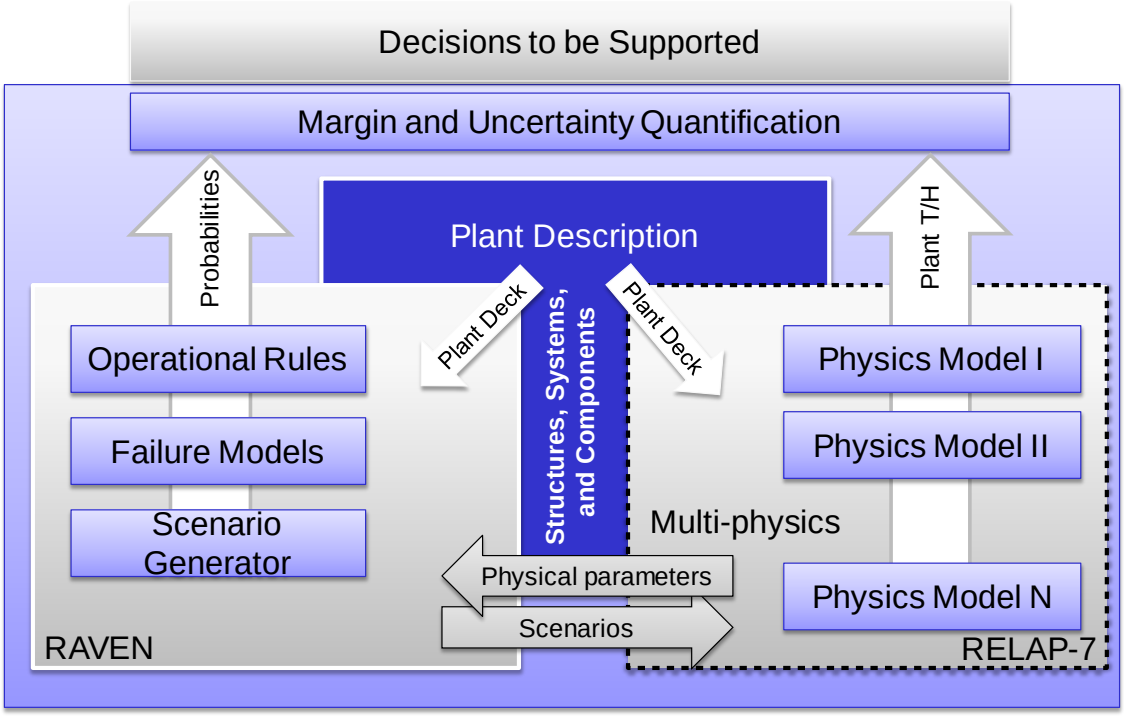

Figure 1-1: The approach used to support RIMM analysis

2. MARGIN MANAGEMENT STRATEGIES

In general, margin management strategies are proposed alternatives (i.e., changes to system, structures, components, or plant procedures) that work to control margin changes due to aging or plant modifications. Alternatives that off-set, or mitigate, reductions in the safety margin are known as margin recovery strategies.

It is intended that RIMM will support a variety of safety margin decisions, including recovery of or increasing safety margins. For example, if core power levels are increased, then plant owner/operators would need to consider implications to the safety margins and possible recovery strategies. It is within this application that we formulated the boiling water reactor (BWR) station black-out (SBO) case study that is described in this report.

2.1 Structure of this report

This report is structure as follows:

- Section 3 presents a detailed description of the BWR Mark I system
- Section 4 shows the structure of the probabilistic risk assessment (PRA) model for a BWR loss-of-offsite (LOOP) plus SBO case
- Section 5 presents in detail the BWR LOOP+SBO case study
- Section 6 shows the results regarding the impact of power uprate on some safety parameters for the LOOP+SBO test case
- Section 7 presents an uncertain analysis performed for the BWR LOOP+SBO case study
- Section 8 compare the results obtained from the PRA models and the ones obtained in Section 6 and 7
- Section 9 summarizes the findings obtained from Sections 6, 7 and 8 and presents the limitations and advancements made as part of this report

3. OVERVIEW OF THE BWR SBO CASE STUDY

3.1 Case Study Purpose

The scope of this case study is to show the capabilities of the RISMC methodology [1] in order to assess limitations and performances of the considered system using a simulation based environment. Such assessment cannot be naturally performed in a classical ET/FT based environment. Hence, we employed the RELAP5-3D [2] thermal-hydraulic (T-H) code and RAVEN [3] as tools to perform a simulation-based stochastic analysis.

3.2 BWR System

The system considered in this test case is a generic BWR power plant with Mark I containment as shown in Figure 3-1. The three main structures are the following:

1. Reactor Pressure Vessel (RPV), it is the pressurized vessel that contains the reactor core.

2. Primary containment includes:

    a. Drywell (DW): it contains the RPV and circulation pumps

    b. Pressure Suppression Pool (PSP) also known as wetwell[1]: a large torus shaped container that contains a large amount of water (almost 1 M gallons of fresh water) and is used in specific situations as ultimate heat sink.

    c. Reactor circulation pumps

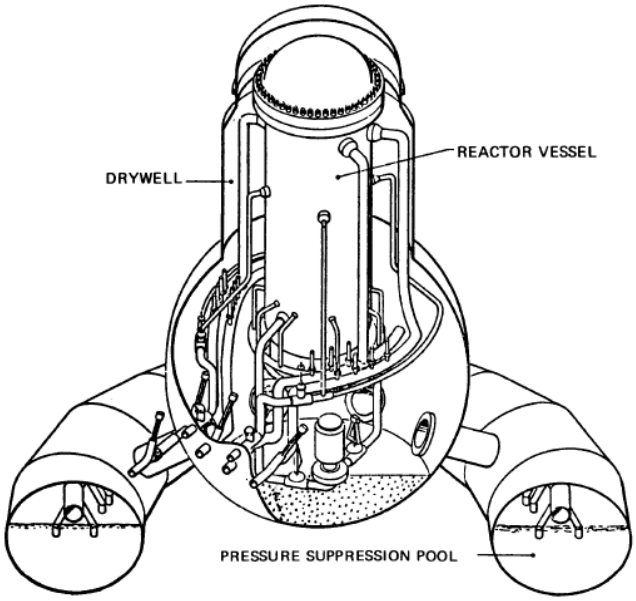

Figure 3-1 View of the BWR Mk.I system

[1] Note that in this report, pressure suppression pool and wetwell indicates the same component

While the original BWR Mark I includes a large number of systems, for the scope of this report and for the test case considered, we will consider a smaller subset of systems:

- RPV level control systems: provide manual/automatic control of the water level within the RPV:

    1. Reactor Core Isolation Cooling System (RCIC): Provide high-pressure injection of water from the CST to the RPV. Water flow is provided by a turbine driven pump that takes steam from the main steam line and discharges it to the suppression pool. Alternatively, the water source can be shifted from the CST to the PSP. Limited water flow can only be provided (600 gpm).

    2. High Pressure Core Injection (HPCI): similar to RCIC but allows much greater water flow rates (5000 gpm)

    3. Low Pressure Core Injection (LPCI): AC powered system that provides water to the RPV when RPV pressure is not pressurized

- RPV pressure control systems: provide manual/automatic control of the RPV internal pressure:

    1. Safety Relief Valves (SRVs): DC powered valves that control and limit the RPV pressure.

    2. Automatic Depressurization System (ADS): separate set of relief valves that are employed in order to depressurize the RPV. RPV depressurization is also referred as RPV blowdown.

- RPV pressure safety valves: this set of safety valves has the scope to keep the RPV pressure below 1105 psi. Activation of these valves is automatic and does not require DC battery.

- Cooling water inventory:

    1. Condensate Storage Tank (CST): the considered BWR plant contains a 375 Kgal of fresh water that can be used to cool the reactor core. In addition, two additional 500 10^3 gal tanks are provided as additional fresh water sources. The alignment of these two tanks to the RCIC/HPCI inlet cannot be performed automatically and requires operator actions.

    2. PSP water: PSP contains a large amount of fresh water (about 1 10^6 gal) that is used to provide ultimate heat sink when AC power is lost.

    3. Firewater system: water contained in the firewater system can be injected into the RPV when other water injection systems are disabled and when RPV is depressurized.

- Reactor operators and staff

- Power systems:

1. Power grids: 2 power grids, 500 KV (main) and 161 KV (secondary), are connected to the plant station thorough two independent switchyards. Both power grids and switchyards provide AC power to the emergency and auxiliary systems of the BWR plant. Loss of power from both switchyards disables the operability of all system except: ADS, SRV, RCIC and HPCI (which require only DC battery).

2. Electrical busses: a series of electrical buses (4160 V and 480 V) and step-down transformers (from 4160 V to 480 V) provide AC power to auxiliary and emergency systems including the LPCI

3. Diesel generators (DGs): emergency AC power is provided by a set of diesel generators that energize the 4160 V buses. DG supply is designed so that emergency AC power can be provided for 24 hours.

4. Battery systems: instrumentation and control systems need DC power (250 VD). DC power is normally provided by AC/DC converters that are connected to the 4160 V busses. In case the 4160 V busses are not energized, emergency DC power is provided by a set of batteries. At nominal conditions, life of this set of batteries is on average 4 hours.

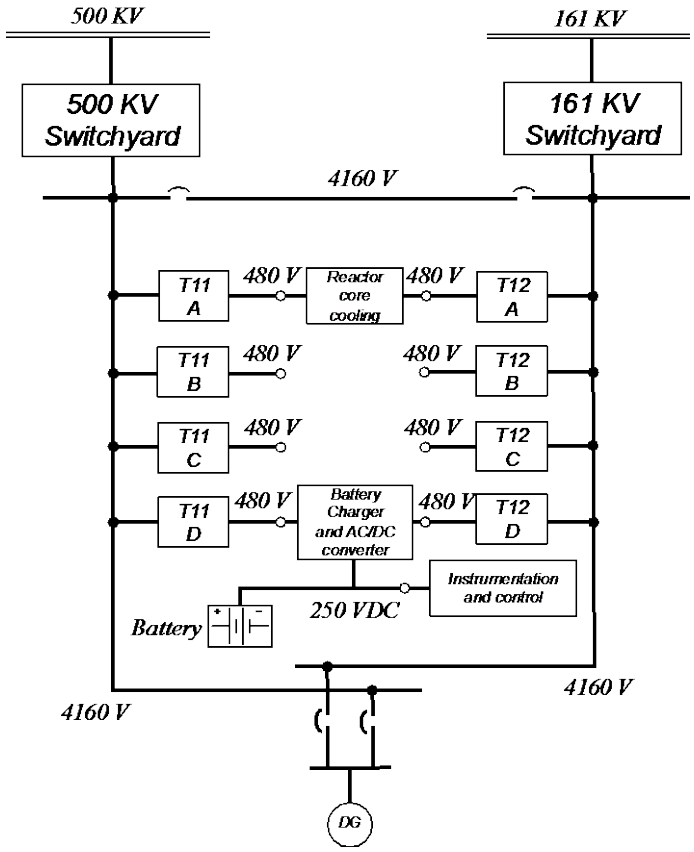

Figure 3-2: Electrical scheme for the BWR SBO test case

3.2.1 RCIC and HPCI

In the absence of AC power, high-pressure water injection from the CST to the RPV is provided by two independent systems: RCIC and HPCI. Water flow injection is provided by a turbine driven pump; steam from the main steam line is used to run the turbine which is then discharged into the PSP. RCIC has a limited flow rate capacity (600 gpm), while HPCI can deliver a much higher water flow rate (5000 gpm). However, for most of the scenarios we observed, the RCIC is sufficient to supply water within the RPV.

Such high-pressure water injection is guaranteed only for RPV pressure ranges between 150 psig and 1120 psig. Pump power is dependent on the pressure inside the RPV and it varies between 500 hp at 1120 psig and 80 hp at 225 psig.

New emergency operating procedures allow the operator to reach a final pressure of 150 psig after ADS activation so that high-pressure water injection can be performed using RCIC/HPCI. In this report, we will not consider this type of scenario and ADS activation will be such that the final RPV pressure is such to allow injection of firewater (below 100 psi).

While AC power is not needed, DC power is required in order to monitor and control the RCIC. Thus, when DC power is lost, high-pressure injection through RCIC/HPCI is also disabled. However, the reactor operator and the plant staff may maintain control of RCIC/HPCI for an additional time by manually opening/closing the RCIC/HPCI steam control valves.

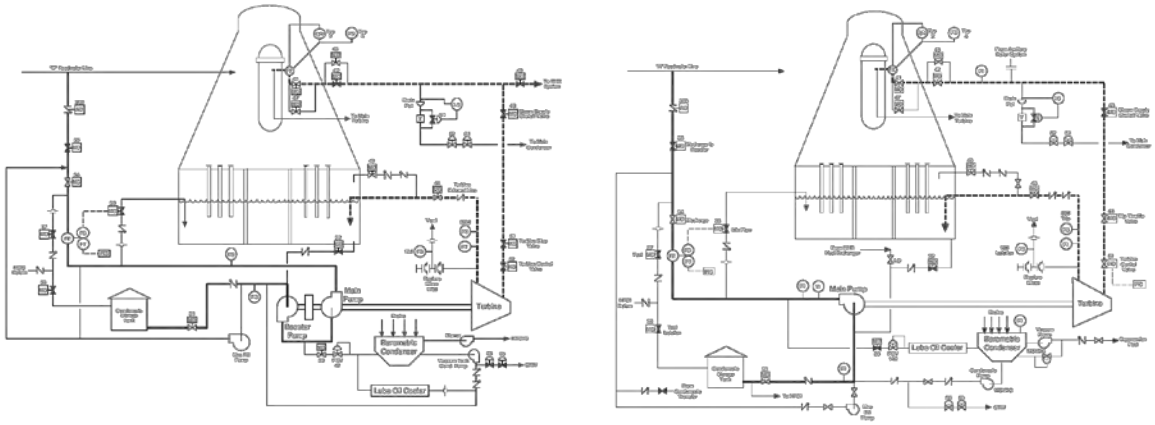

Figure 3-3: RCIC (left) and HPCI (right) schemes

3.2.2 BWR Containment limitations

In an accident scenario, the set of emergency operating procedures requires the reactors operators to monitor not just the RPV but also the containment (both DW and PSP) thermo-hydraulic parameters (level, pressure and temperature). In particular, a set of limit curves is provided so that when they are crossed, the operators are required to activate the ADS system. These limit curves, also known as Heat Capacity Temperature Limits (HCTL), are shown in Figure 3-4 for PSP (top figures) and DW (bottom figure).

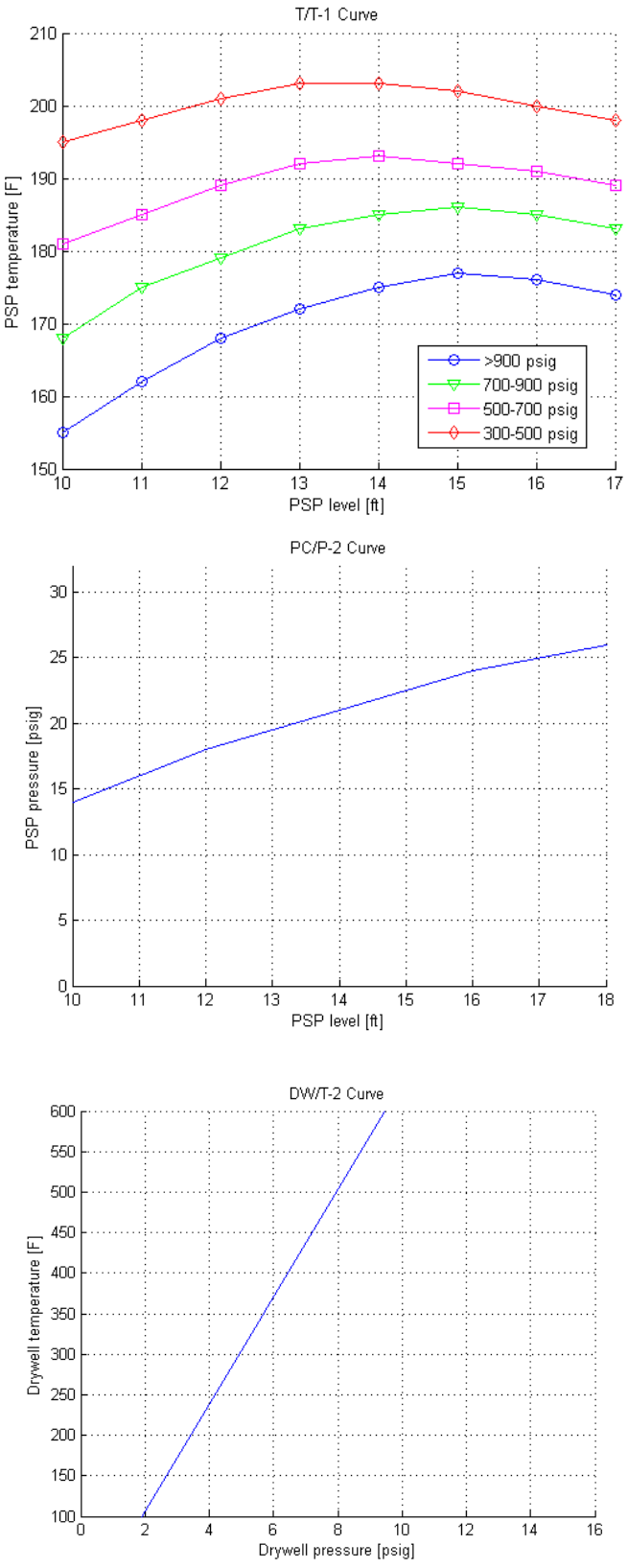

Figure 3-4: HTCLs for PSP (top and middle) and DW (bottom)

3.2.3 Pump Seals

The two circulation pumps that provide water flow in the RPV during normal operation require a constant flow of cooling water to keep the pump seals cooled. This cooling is provided by the Component Cooling Water (CCW) and the Service Water (SW) systems. When AC power is not available, then the CCW system is disabled and the high pressure and temperature values of the water in the RPV may cause the seal to fail. When this happens, a loss of cooling accident (LOCA) from the seal may occur in the drywell[2]. From BNL-NUREG- 49115 it was possible to obtain typical values of flow rates of seal LOCA:

- Expected water leakage flow rate: 18 gpm (4 m^3/h) per pump
- Maximum water leakage flow rate: 100 gpm (45.4 m^3/h) per pump

Note that, since the BWR system considered is composed of two pumps, overall water leakage flow rate is doubled.

3.2.4 RCIC/HPCI Alternate System Alignments

During a SBO condition, the operator cycle SRVs in order to keep RPV pressure between 900 and 1100 psi. Steam released by SRV is dumped into PSP and, thus, both the PSP water level and temperature increases with time. If such water injection is protracted for a long time, then the PSP water level can reach an addition limit: the T/L-1 limit curve (see Figure 3-5). When PSP water level limit is reached, then the operators are required to switch the RCIC/HPCI suction from the CST to the PSP.

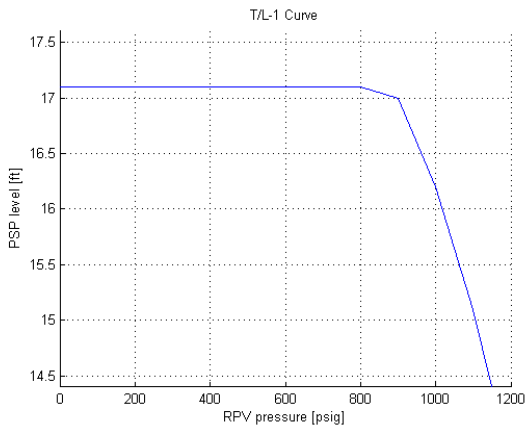

Figure 3-5: Plot of the T/L-1 curve

3.2.5 Firewater system

As a last emergency measure to provide cooled water in the RPV, the reactor operators can use the plant firewater system. Such system is characterized by a large water flow rate, i.e. 2500 gpm, and a discharge pressure of 120 psi. After activation of the ADS, the RPV pressure is assured to be below 150 psi so that, when available, the reactor operator will be able to inject water inside the RPV through the firewater system.

---

[2] Typically, seal LOCA are more often considered in PWR systems rather than BWRs due to much higher pressure values inside the RPV. However, the ET structure in the BWR SPAR model considered explicitly queries the status of the seal of the recirculation pumps. Thus, we included seal LOCA leakages into our analysis.

The alignment of the firewater system to the RPV water inlet is, however, not an easy task and depending on the plant conditions (no illumination, large amount of debris in the surrounding area) this may take hours.

3.3 BWR SBO Scenario

The accident scenario under consideration is a LOOP followed by loss of the DGs, i.e. SBO initiating event. In more details (see Figure 3-6 and Figure 3-7):

- At time t = 0: the following events occur:
  - LOOP condition occurs: due to external event, the 500 KV line de-energize and the switchyard connected to the 161 KV line gets damaged
  - LOOP alarm triggers the following actions:
    - Operators successfully scram the reactor put it in sub-critical conditions by fully inserting the control rods in the core
    - MSIVs successfully close and isolate the primary containment from the turbine building
    - Emergency DGs successfully start and the 4160 V busses are kept energized
    - Decay heat generated by the core is removed from the RPV through the RHR system
    - DC systems (i.e., batteries) are functional
- SBO condition occurs: due to internal failure, the set of DGs fails and the 4160 busses de-energize. Removal of decay heat is impeded. Reactor operators start the SBO emergency operating procedures and perform:
  - RPV level control using RCIC or HPCI
  - RPV pressure control using SRVs
  - Containment monitoring (both drywell and PSP)
- Plant staff start recovery operations to bring back on-line the DGs while the recovery of grid power is underway by the grid owner emergency staff
- Due to loss of AC power, the Component Cooling Water (CCW) and Service Water (SW) systems cannot provide cooling for the seal of the circulation pumps. The overheating of these seals can cause their failure causing release of water from the RPV to the drywell (pump seal LOCA)
- Due to the limited life of the battery system and depending on the use of DC power, battery power can deplete. When this happens, all remaining control systems are offline causing the reactor core to heat until maximum temperature limit for the clad is reached: core damage (CD) condition occurs

- If DC power is still available and one of these condition are reached:
    - Failure of both RCIC and HPCI
    - HCTL limits reached
    - Low RPV water level

  then the reactor operators activate the ADS system in order to depressurize the RPV and allow firewater injection, if available[3].

- When pressure within the PSP reaches 70 psi, then the reactor operators are authorized to vent the containment in order to maintain containment integrity

- When AC power is recovered, through successful re-start/repair of DGs or off-site power, RHR can be now employed to keep the reactor core cool

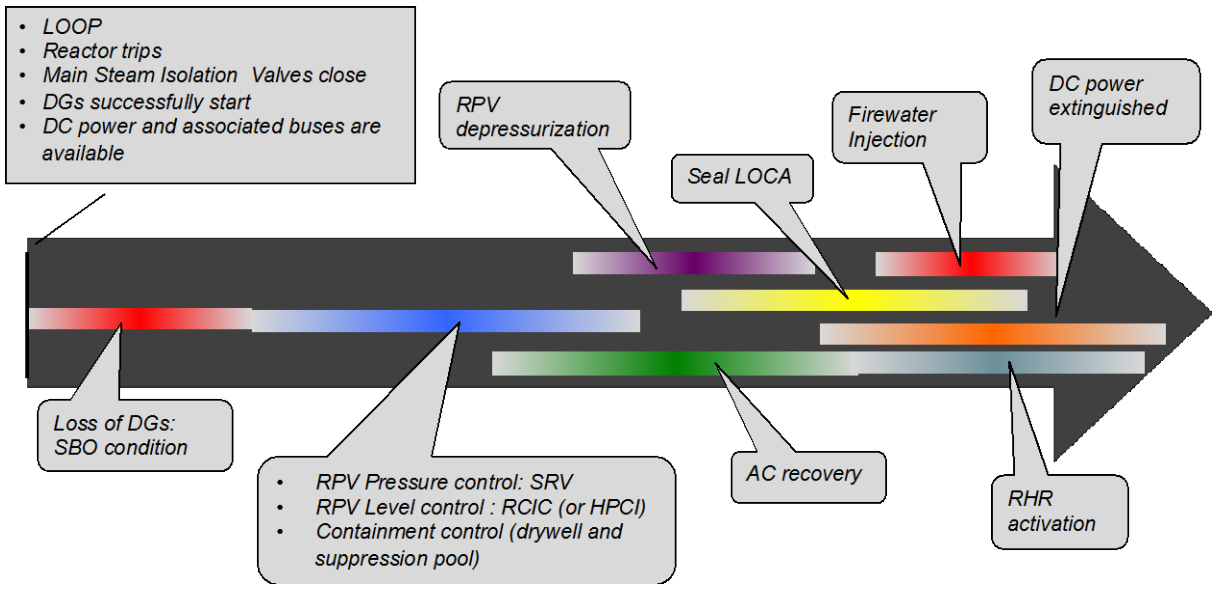

Figure 3-6: Sequence and timing of events for the BWRO SBO test case

[3] Two different ADS strategies can be followed for BWR systems:

1. Complete opening of all ADS relief valves and full RPV depressurization. Typically, the depressurization is complete within minutes
2. Controlled RPV depressurization performed by cycling a single SRV with the scope to reach 125 psi in the RPV such that both RCIC and HPCI can still be used in case firewater injection is not available. Such depressurization may take about 80 minutes. However, this controlled depressurization can be performed much before the heat capacity curve for the PSP is reached.

   For the scope of this research work we have decided to employ only the first ADS strategy in order to keep a model consistent with BWR SBO model contained in the PRA.

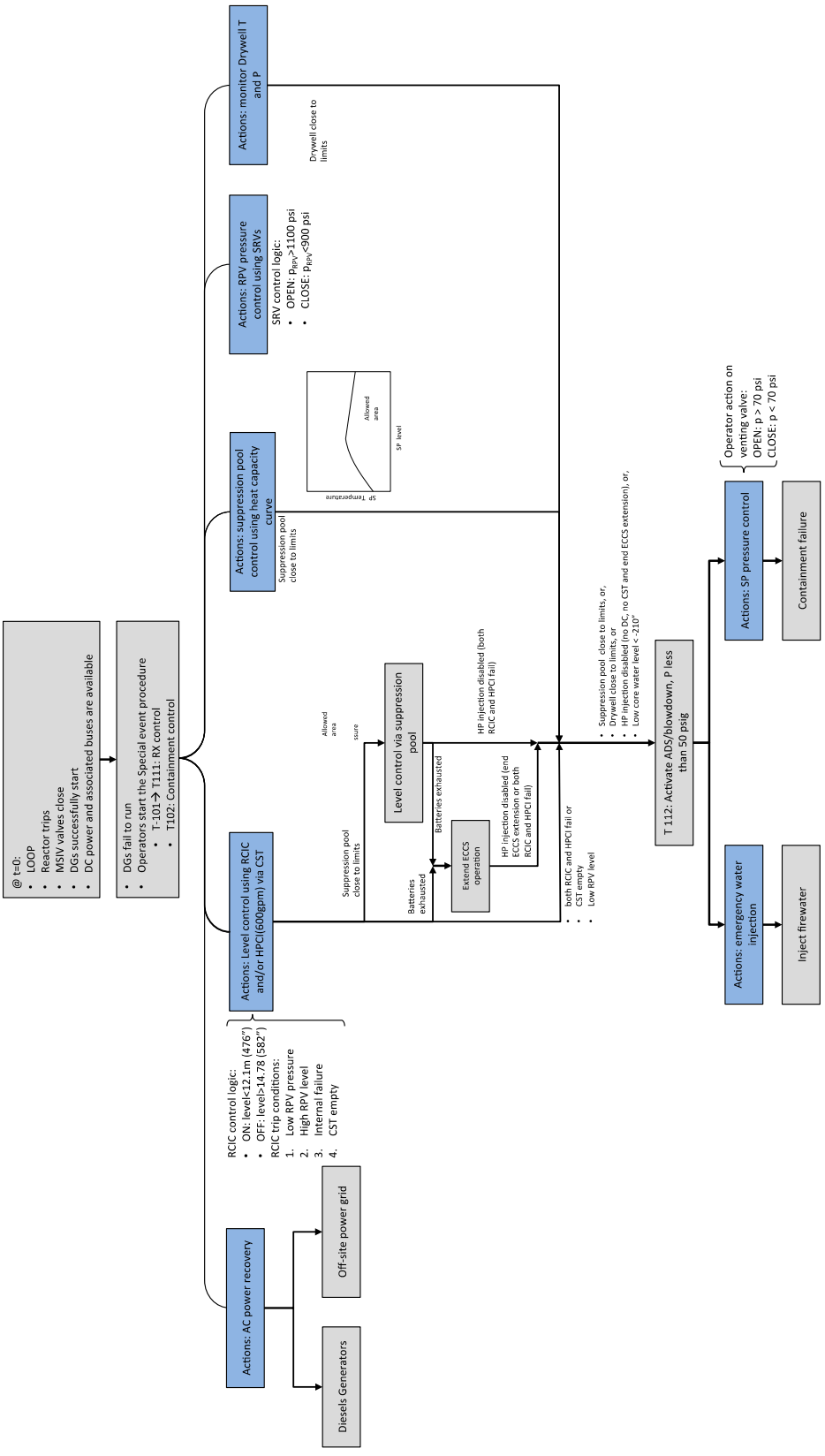

Figure 3-7: Scheme of the control logic for the BWR SBO test case

3.4 Stochastic Parameters

The choice of the set of stochastic parameters to consider in the analysis was based on the preliminary PRA model results obtained for a typical BWR SBO case. For all basic events (e.g., DG fail to run) we have considered the following indexes:

- Fussell-Vesely importance
- Birnbaum importance
- Event-tree structure for a LOOP-SBO

The most relevant basic events obtained from the PRA model are listed in Table 3-1

Table 3-1: Basic Events obtained from the PRA model

1	*Failure time of DGs*	*5*	*Offsite AC power recovery*
2	*Recovery time of DGs*	*6*	*HPCI fails to run*
3	*Battery life*	*7*	*RCIC fails to run*
4	*SRV stuck open*		

In addition we also looked into the SPAR-H [4] usage in the PRA models in order to include timing/sequencing of events associated to human actions. In this respect, we have identified 5 actions that are listed in Table 3-2:

1. Manual ADS activation: operator manually depressurizes the RPV by activation the ADS system after HCTL limits are reached
2. Extended ECCS operation: operators may extend RCIC/HPCI and SRVs control even after the batteries have been depleted. This action actually summarizes two events:
    a. Operators manually control RCIC/HPCI by acting on the steam inlet valve of the turbine
    b. Operators supply DC power to the SRVs through spare batteries
3. Containment (PSP) venting: when PSP reaches a pressure of 70 psi, reactor operators can vent the containment in order to maintain containment integrity
4. Firewater injection: as an emergency action, when RPV pressure is below 100 psi plant staff can connect the firewater system to the RPV in order to cool the core and maintain an adequate water level. Such task is, however, hard to complete since physical connection between firewater system and RPV inlet has to made manually

5. Increase CST capacity: original CST capacity is 375 Kgal. In addition, two more tanks having 500 Kgal capacity each can be used. The action to switch from CST to these two additional tanks can be performed when CST level is low.

Table 3-2: Human interventions obtained from SPAR-H model

1	*Manual ADS activation*	*4*	*Firewater injection*
2	*Extended ECCS operation*	*5*	*Increase CST capacity*
3	*Containment (SP) venting*		

Ultimately, we also included uncertainties associated with five additional parameters listed in Table 3-3.

Table 3-3: Set of addition stochastic paramaters considered

1	*Clad damage temperature*	*4*	*Containment failure pressure*
2	*Seal LOCA start time*	*5*	*Reactor power*
3	*Seal LOCA flow rate*		

4. STATIC PRA ANALYSIS

One of the insights we wanted to derive as part of the initial BWR SBO modeling activity is to perform a comparison of the static PRA approach with the RISMC methodology. In this section, we briefly describe the static PRA approach in order to inform the comparison made later in the report. The ET structure of the PRA model for a BWR SBO consists of the following ETs (see Figure 4-1):

- Loss Of Offsite Power Grid Related (LOOPGR)
- Station Black Out (SBO)
- SBO-1: SBO + 1 SRV stuck open
- SBO-2: SBO + 2 or more SRVs stuck open
- SBO-OP: Off-site power recovery

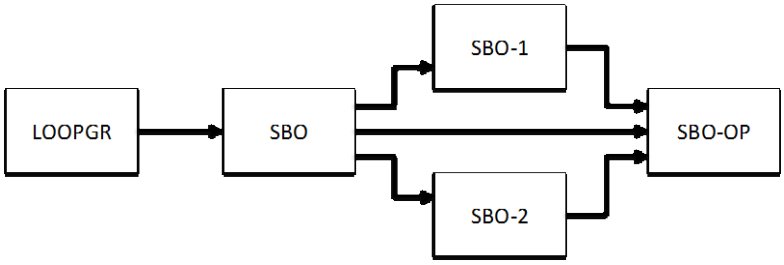

Figure 4-1: ET structure of the LOOPGR+SBO scenario

The LOOPGR ET (see Figure 4-2) starts with a grid related LOOP as initiating event followed by a branch on the success/failure of the reactor shutdown. Then the ET queries the status of emergency power (i.e., diesel generators); a failure of such system leads to a transfer ET: the SBO ET (see Figure 4-3).

In the SBO ET (see Figure 4-3) the following events are queried in sequence:

1. SRV(s) status
2. Pump seal integrity
3. RCIC/HPCI availability
4. Extended ECCS operation
5. ADS activation
6. FW injection
7. Offsite power or DG recovery
8. Containment venting + late water injection

In case one or more SRV (see Figure 4-5) are stuck open the following events are queried in sequence:

1. RCIC/HPCI availability
2. Offsite power or DG recovery

The off-site power recovery ET (see Figure 4-4) queries these events:

1. RCIC/HPCI availability
2. PSP cooling
3. ADS activation
4. Low pressure RPV injection
5. Containment venting + late injection

In this study we will compare the results obtained from the dynamic analysis performed using RELAP-5 and some of the event tree paths generated in the PRA models using the SAPHIRE software.

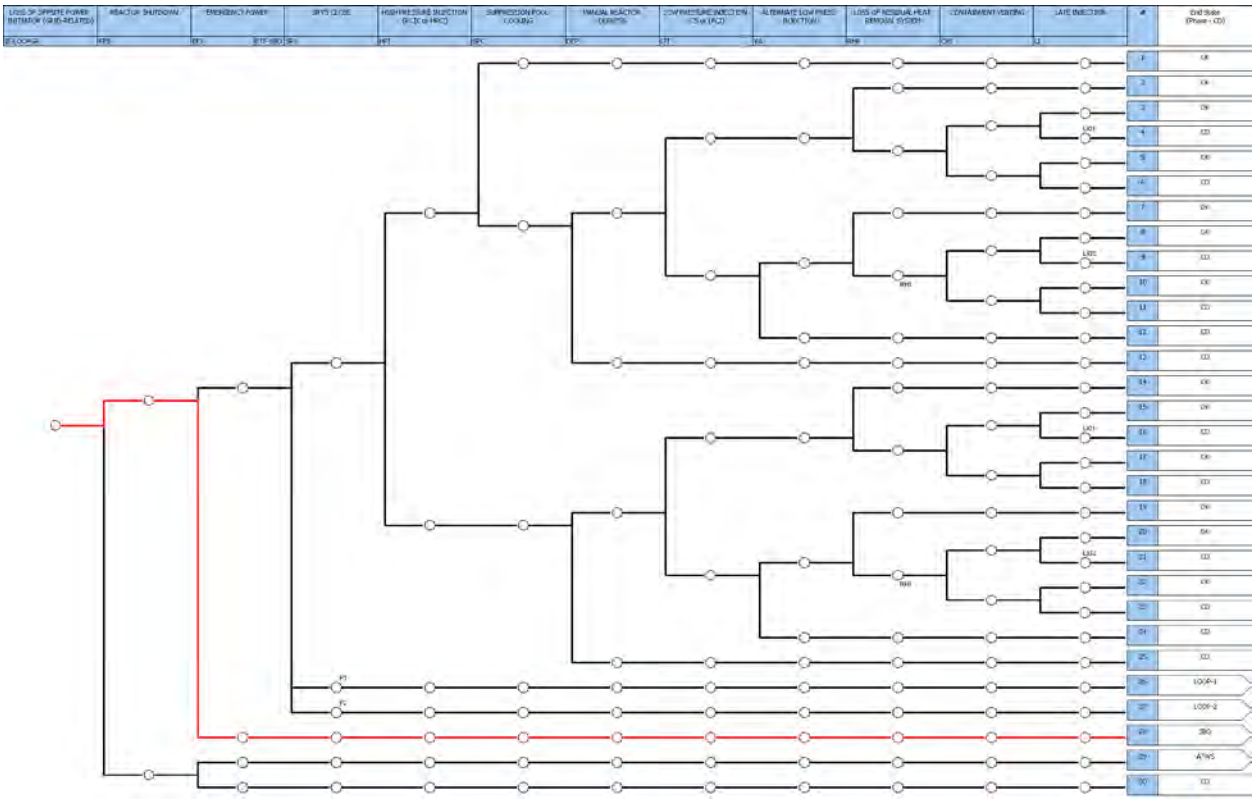

Figure 4-2: LOOPGR Event Tree; path to SBO ET is shown in red

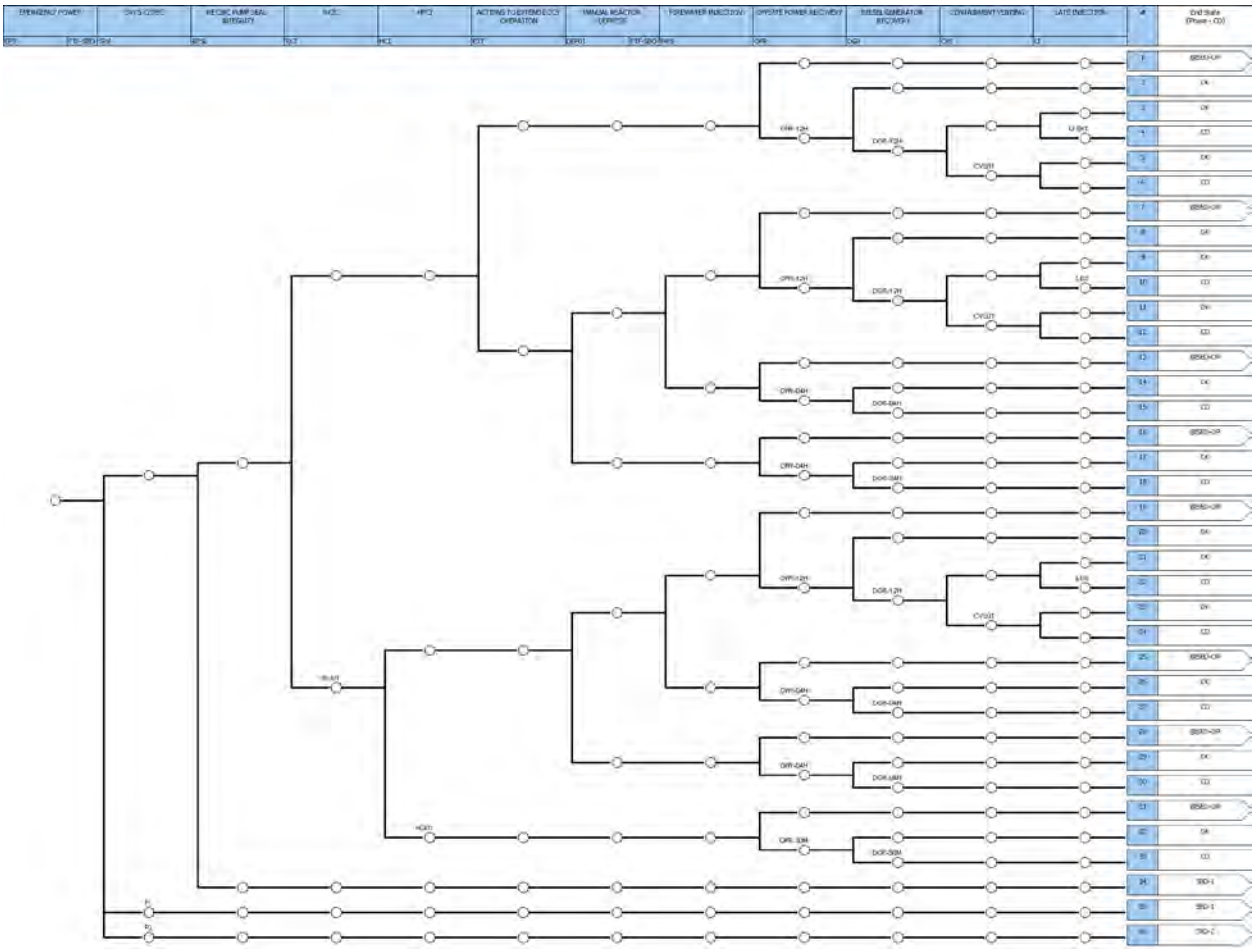

Figure 4-3: SBO ET

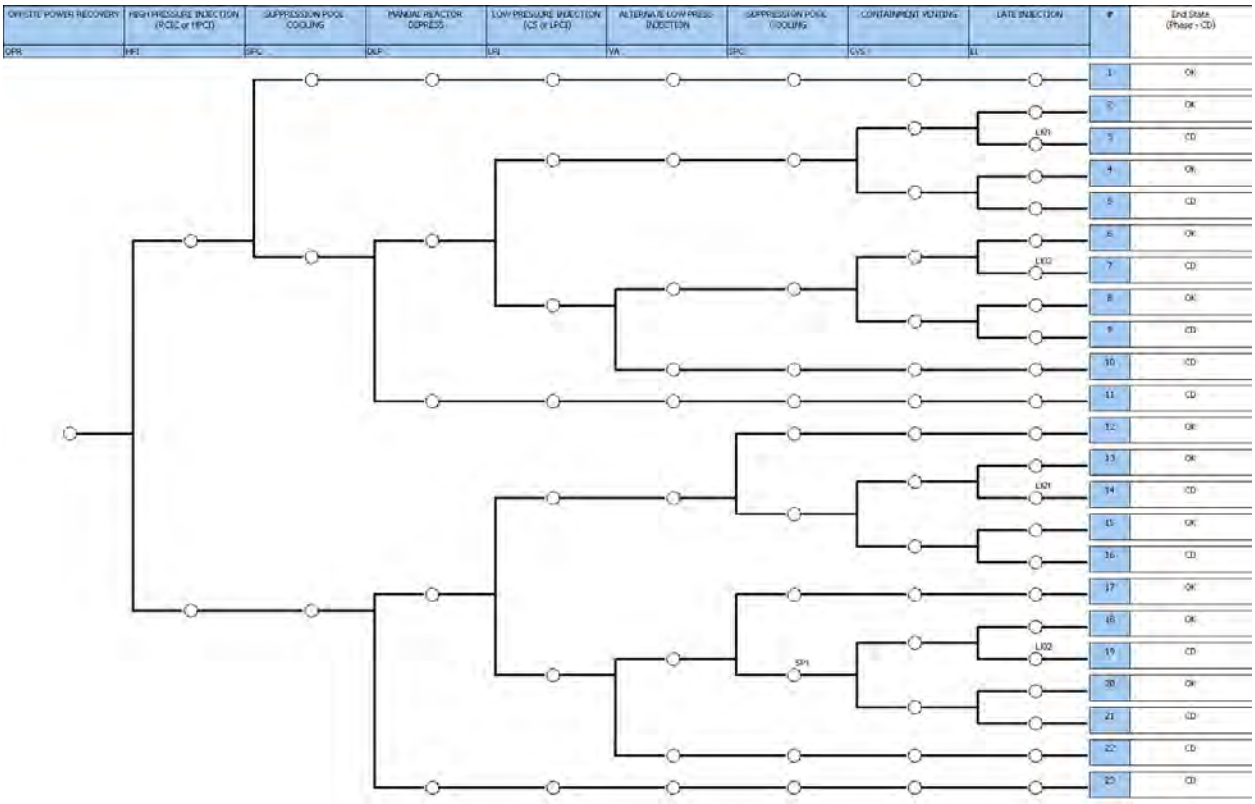

Figure 4-4: SBO-OP ET

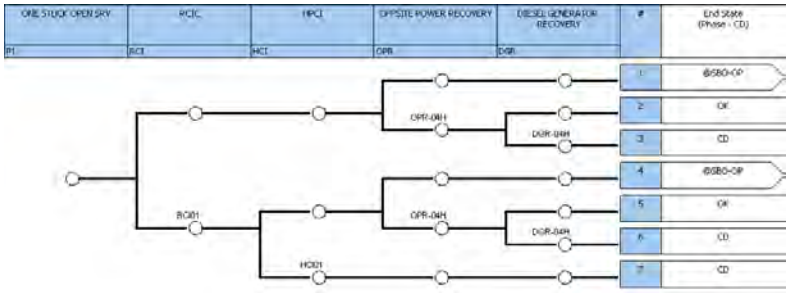

Figure 4-5: SBO-1 ET (SBO-2 ET is identical to SBO-1 ET)

5. CASE STUDY DETAILS

5.1 The Case Study Approach

5.1.1 RISMC Process Steps

The mechanics to conduct margins analysis, including a methodology for carrying out simulation-based studies of safety margin, are described in this section. The steps performed during a RISMC analysis [1] (also shown in Figure 5-1) are listed below:

1. Characterize the issue to be resolved and the safety figures of merit to be analyzed in a way that explicitly scopes the modeling and analysis to be performed.

2. Describe the decision-maker and analyst's state-of-knowledge (uncertainty) of the key variables and models relevant to the issue. For example, if long-term operation is a facet of the analysis, then potential aging mechanisms that may degrade components should be included in the quantification.

3. Determine issue-specific, risk-based scenarios and accident timelines (the key parts of which are illustrated in Figure 5-2).

4. Represent plant operation probabilistically using the scenarios identified in Step 3. For example, plant operational rules (e.g., operator procedures, technical specifications, maintenance schedules) are used to provide realism for scenario generation. Because numerous scenarios will be generated, the plant and operator behavior cannot be manually created like in current risk assessment using event- and fault-trees. In addition to the *expected* operator behavior (plant procedures), the probabilistic plant representation will account for the possibility of failures.

5. Represent plant physics mechanistically. The plant systems-level code is used to develop distributions for the key plant process variables (i.e., loads) and the capacity to withstand those loads for the scenarios identified in Step 4. Because there is a coupling between Steps 4 and 5, they each can impact the other. For example, a calculated high loading (from pressure, temperature, or radiation) in an SSC may disable a component, thereby impacting an accident scenario.

6. Construct and quantify probabilistic load and capacity relating to the figures of merit analyzed to determine the probabilistic safety margin.

7. Determine how to manage uncharacterized risk. Because there is no way to guarantee that all scenarios, hazards, failures, or physics are addressed, the decision maker should be aware of limitations in the analysis and adhere to protocols of "good engineering practices" to augment analysis.

8. Identify and characterize the factors and controls that determine safety margin in order to propose Margin Management Strategies. Determine whether additional work to reduce uncertainty would be worthwhile or if additional (or relaxed) safety control is justified.

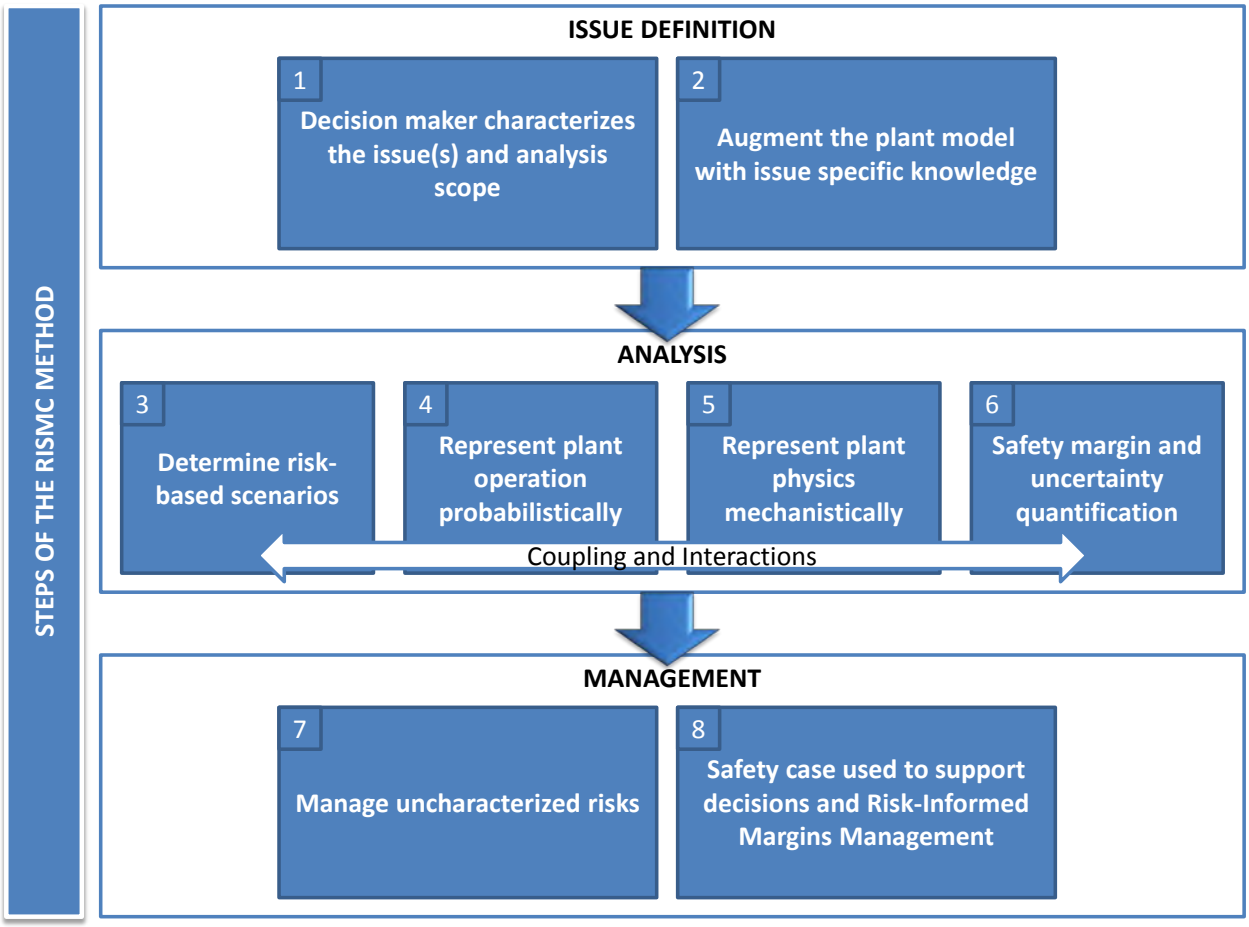

Figure 5-1. Depiction of the high-level steps required in the RISMC method [1].

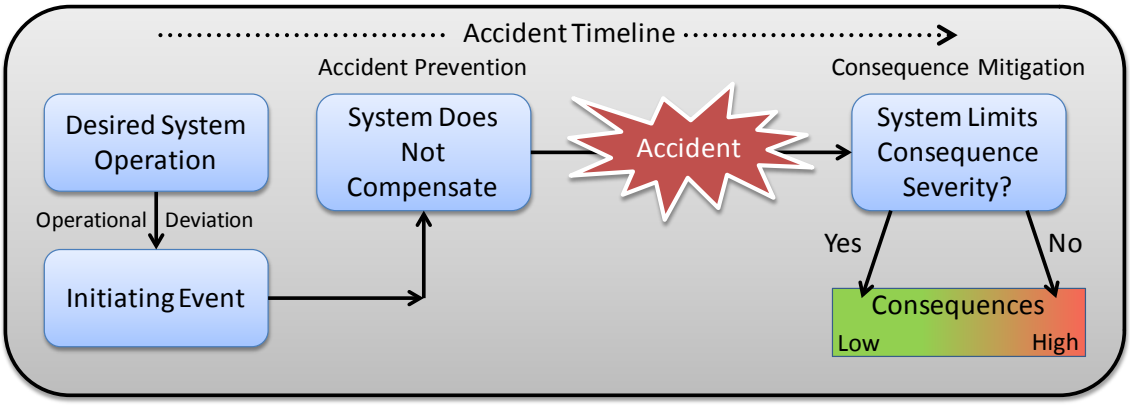

Figure 5-2. Accident scenario representation

5.2 Mechanistic Plant Modeling

5.2.1 RELAP-5 system model

The BWR dynamic has been modeled using RELAP-5. The system nodalization is shown in Figure 5-3 and it includes:

- RPV components such as the reactor core, down-comer, steam dome, jet-pump, SRVs, ADS
- Containment component such as PSP, drywell, recirculation pumps and CST
- External systems such as RCIC, HPCI, firewater

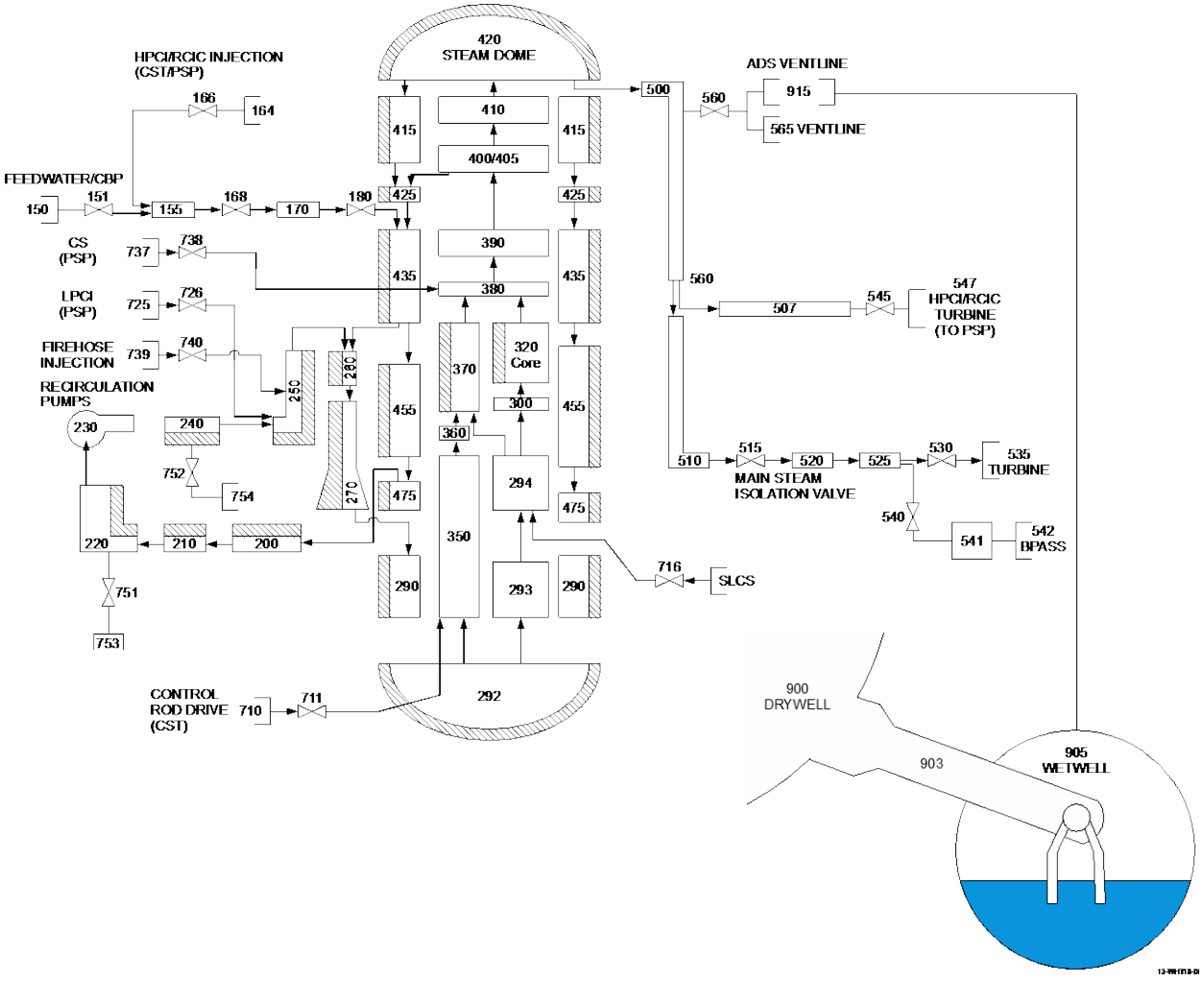

Figure 5-3: RELAP-5 nodalization scheme for the BWR system

For the scope of this analysis we have decided to stop the simulation when one these three stopping conditions are met:

1. Clad temperature reaches failure temperature
2. AC power recovered
3. Firewater available
4. PSP pressure reached failure pressure

5.2.1.1 RCIC/HPCI and SRVs Control Logic Implementation

The primary logic sought after in this model was the previously discussed Containment Heat Capacity curves, Safety Relief Valve (SRV) control logic, and the Reactor Core Isolation Cooling (RCIC) and High Pressure Coolant Injection (HPCI) systems. The SRV set-points are for the SRVs to open at 1100 psia and close at 900 psia, and the HPCI/RCIC set-points are to engage when the core is below 39.67' of water in the pressure vessel and shut off when the core is above 48.5' of water. These set-points are designed to keep the core in a stable and cooled configuration.

Specifically, the way these setups work, logically, is that we use a “true test” trip to determine whether the SRVs are currently open or HPCI/RCIC is flowing, as the case may be. When the simulation is engaged, and we are in between the two set-points, nothing happens until we exceed either the upper or lower set-point, which will toggle the state of the system - in case of the SRV high set-point, it opens the SRVs to lower the pressure vessel pressure until it hits the low set point, when the SRVs will close to increase the pressure vessel pressure, and so cycling between the two set-points.

5.2.1.2 Pump Seal LOCA Modeling

Pump Seal LOCA modeling was accomplished using a valve attached to the outlet volume of the pump component. Due to RELAP5 limitations, the valve cannot be attached directly to the pump component, and the outlet side was chosen over the inlet side due to physical considerations – it is more realistic to have water that has just exited the pump being vented than to have water that has never reached the pump being vented when attempting to emulate a Pump Seal LOCA.

The leak valve was attached to the outlet volume of the recirculation pump component on one side, and to a single volume “pipe” on the other side, which connected to the drywell. The extra component was necessary to line up the connections appropriately – otherwise the heights of the two connections were not the same, a non-physical scenario. The volume of the extra component was compared to the volume of the drywell component and found to be negligible, and did not impact results for the DW pressure and temperature in non-Pump Seal LOCA scenarios.

5.2.1.3 PSP Modeling

Two attempts have been made to model the PSP, each with their own advantages and disadvantages. The first attempt to model the PSP was done using a single volume component, under the assumption that the violent injection of steam into the torus would cause it to be a well-mixed volume. The advantages of this are that it is computationally fast and seems to model the temperature and level in the Torus very well. The disadvantage is that it has been difficult to procure reasonable pressure results, which has been deemed less important than precise temperature results.

The second attempt to model the PSP was done using a ten-volume "pipe" component. It more accurately models the temperature of the PSP, but it has problems modeling the level of the PSP; in addition, it is computationally slower than the single volume PSP model, and more prone to crashing[4].

We decided to use the first (single volume) model, since PSP temperature and level are the most important variables to be considered in the analysis.

5.2.1.4 Containment Heat Capacity Curves

The Containment Heat Capacity Curves were implemented by breaking each curve into a adequate number of linear segments, finding appropriate equations for those linear segments, and then using control variables, trips, and logic gates to model, watch, and links together these linear segments into full curves.

For clarity, when examining the results of the models, the control variable for each linear segment (if the equation for the segment $Y < MX+B$ is safe) is modeled as $Y-MX-B$; by doing this, it is easy to track how close we are to violating the curve – the more negative the control variables are, the safer we are. When any of the Containment Heat Capacity Curve control variables become positive, appropriate action (such as, for example, activation of the ADS) is taken.

5.2.1.5 RCIC/HPCI switch from CST to PSP

According to the system control logic (see Figure 3-7), operators have to switch suction from the CST to the PSP when safe limits of Torus Level versus Pressure are exceeded. This action is done much the same way as the rest of the Containment Heat Capacity Curves are modeled – the curve is broken into linear segments and modeled with control variables. When the curve is exceeded, the inlet valve that connects the CST to HPCI/RCIC is closed and the inlet valve that connects the PSP to HPCI/RCIC is opened.

However, this is not expected to ever be necessary since the PSP level increases very slowly, and the PSP temperature increases relatively quickly. Thus, it is expected that the ADS will activate, caused by a trip on PSP temperature, long before HPCI/RCIC suction is changed from the PSP to CST.

[4] During a sensitivity analysis of PSP initial water level, many crashes occurred with the ten volumes pipes model of the PSP. The single volume model of the PSP, on the other side, greatly reduced such number of codes crashes.

5.2.1.6 Decay Heat Curve

The original implementation of the decay heat power in RELAP5 was built by using Point Kinetics Equations for the decay heat. However, due to the nature of the problem - namely that sometimes the DGs would operate for some time after LOOP, we needed a way to start the simulation directly when SBO condition occurs. This requires computing corrections to the temporal profile of decay heat power (adjusted to start not when LOOP condition occur but when DGs fail to run.)

To accomplish this, the model was modified by determining the RELAP5 decay heat power temporal curve and by inserting it as a table in the model input file.

5.2.1.7 Batteries

In the simulation, the set of batteries are modeled with a simple timer: turning off HPCI/RCIC and closing any open SRVs (excluding ones that have become stuck open) once the timer is up. This was done, in part, because modeling the power demands of the plant was deemed overly complex when it can be effectively replicated with a battery lifetime probability distribution. Once battery power is up, the model generally ends by core damage unless AC power is restored in the short window of time between loss of battery power and core damage.

5.2.1.8 Example of Scenario Dynamics

We performed several tests of the BWR input file in order to:

- Check the system overall control logic
- Make sure that the temporal behavior of the system state variables had a physical meaning
- Decrease the chance of simulation crash

An example of scenario is shown in Figure 5-4:

- Following a failure to run of DGs, RPV pressure increases while RPV water level decreases. This triggers activation of both RCIC and SRVs.
- Cycling of SRV causes the PSP temperature to increase at each SRV activation
- RCIC activation causes RPV pressure to drop and RPV level to increase
- Loss of DC battery causes the impossibility to control both RPV level and pressure. While RPV level decreases, pressure is kept steady at around 1105 psi due to continue cycling of the RPV safety valves (automatic activation for RPV pressure greater than 1105 psi)

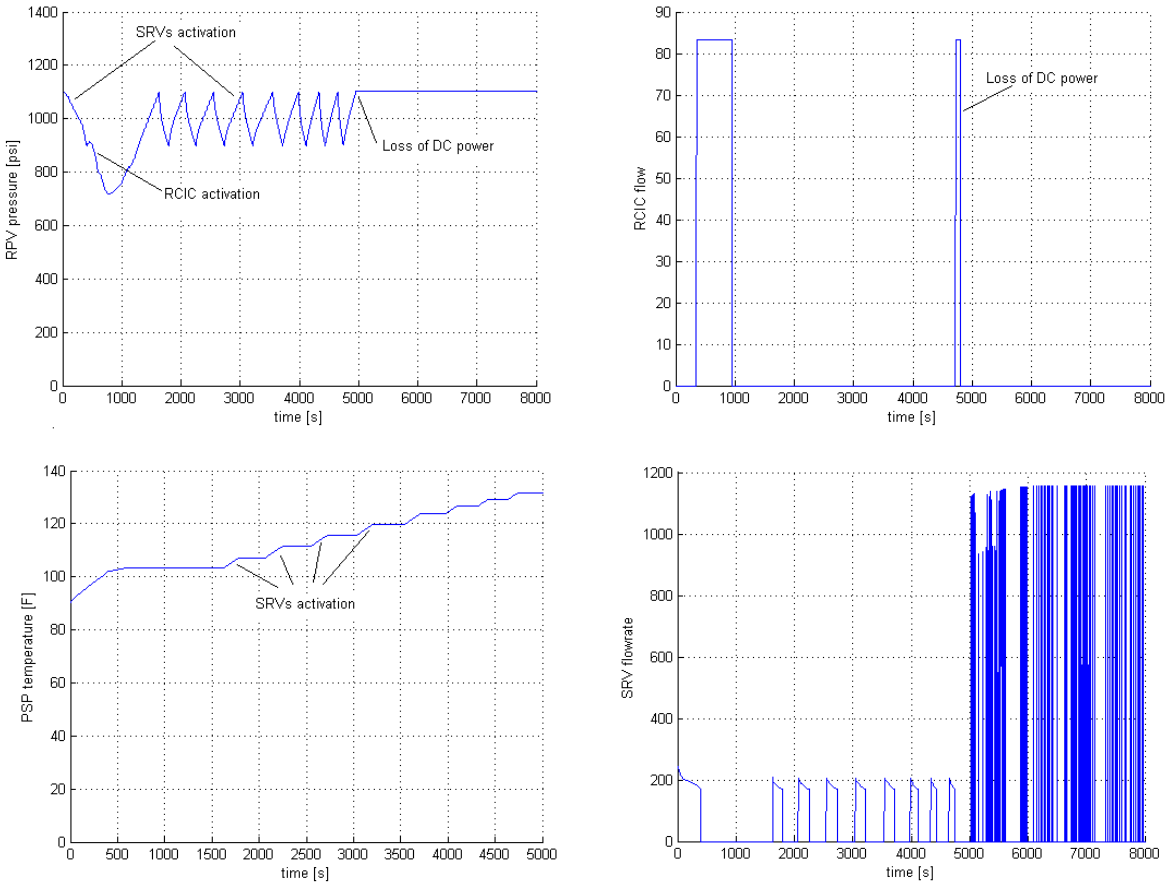

Figure 5-4: Example of BWR SBO scenario

5.2.2 RELAP-7 system model

Two-phase flow modeling capability has been developed in the RELAP-7 code, aimed at demonstrating simulation of a BWR with simplified geometries under extended SBO transient conditions. A number of components developed for single-phase pressurized water reactor model analysis (such as Pipe and Core Channel) have been extended to include two-phase flow modeling capability. Additionally, a set of new components have been developed, including the Separator Dryer, Down Comer, Valve, Turbine, and Wet Well components. A full seven-equation, two-phase model has been implemented into RELAP-7 and the results have been demonstrated with a few components – this capability will be expanded during the software development in FY2014.

For the RELAP-7 BWR model, we used the system shown in Figure 5-5. As part of the accident scenario simulation, we looked at cases where safety injection does not function and cases where cooling water is injected (via RCIC). For the first case (no safety injection), results from RELAP-7 indicate that core damage will occur in a little more than one hour after the SBO – this result is shown in Figure 5-6 (where we also compare the MELCOR SBO calculation done for Peach Bottom as part of NUREG-1953). Note that additional details of RELAP-7 SBO analysis can be found in reference [5].

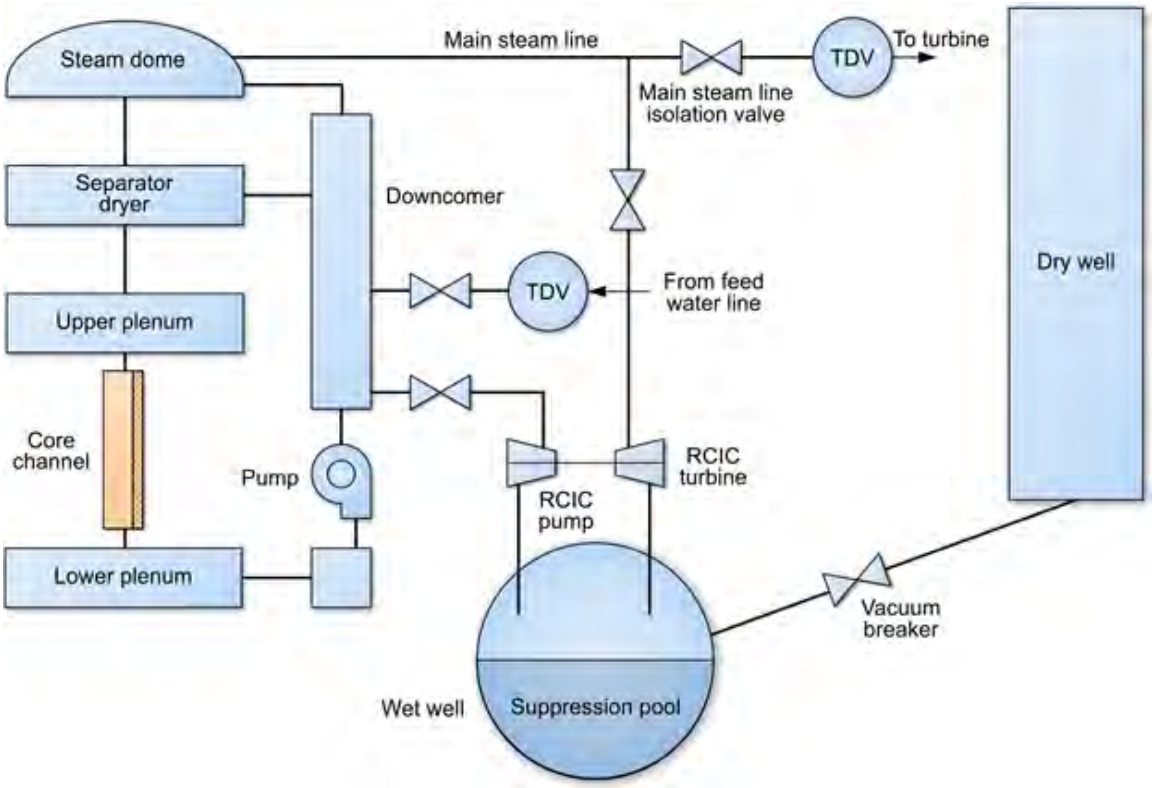

Figure 5-5. Schematics of a simplified BWR system.

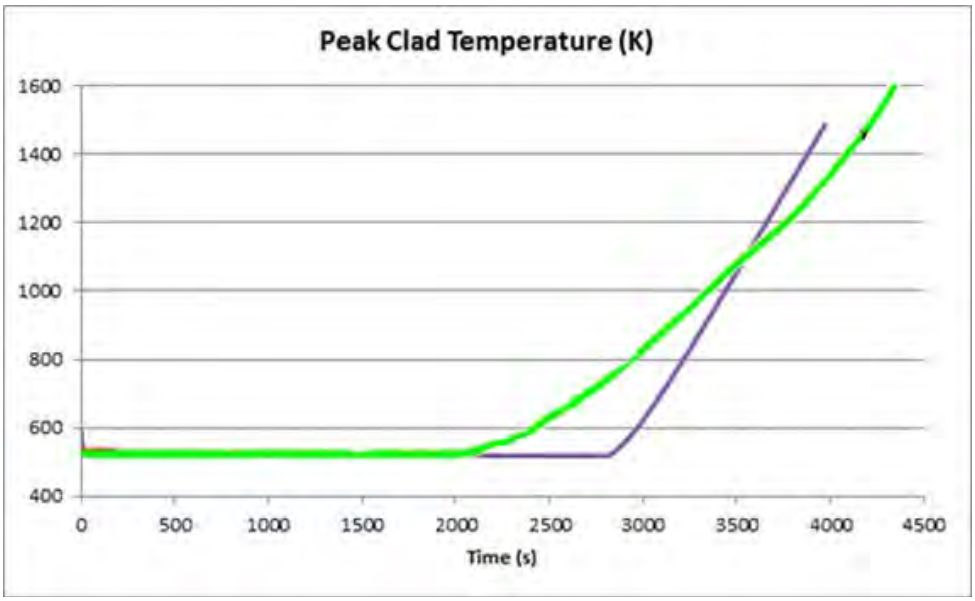

Figure 5-6. RELAP-7 calculated peak clad temperature during SBO with no injection.

5.3 Probabilistic Plant Modeling

5.3.1 Pump Seal LOCA Modeling

As indicated in Section 3.2.3, pump seal LOCA occurs for high values of temperature and pressure of the water in the RPV. Due to lack of both data and models we were not able to build a detailed model that would estimate the likelihood of seal LOCA as function of the RPV water temperature and pressure (by using, for example, a Larson-Miller correlation [6]). For our scope we are interested in the timing of occurrence for such events and the water flow rate leaking from the seal.

We decoupled these two parameters (i.e., time at which seal LOCA occurs and leakage flow rate) by characterizing them with two independent distributions. For the seal LOCA leakage rate, the values indicated in BNL-NUREG-49115 [7] suggested that the lognormal distribution having mean value of 18 gpm and standard deviation of 0.6 gpm (see Figure 5-7) might be a good representation of this phenomenon.

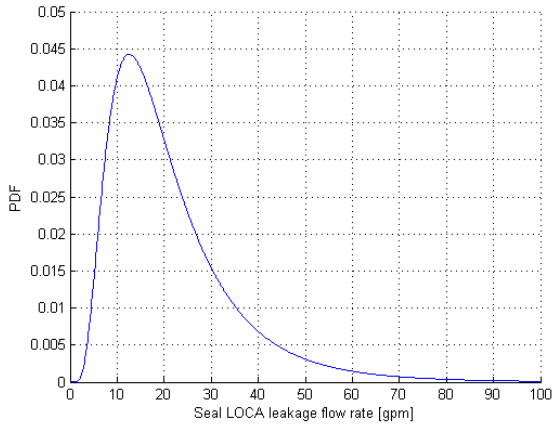

Figure 5-7: PDF for seal LOCA flow rate

Unfortunately our literature research did not provide us with values regarding the time at which such leakages would occur. In the total absence of data, we chose to simply characterize such event with a uniform distribution bounded between 0 and 12 hours after the beginning of the SBO condition. This allows us to evaluate the impact of seal LOCA timing on system evolution.

5.3.2 Human interventions

The probabilistic modeling of the five human interventions listed in Table 3-2 was done by looking at the SPAR-H model from a generic BWR PRA. In general, SPAR-H characterizes each operator action though eight parameters – for this study we focused on the three most important factors:

- Stress/stressors level
- Task complexity

- Time available to perform such task

These three parameters are used to compute the probability that such action will happen or not; such probability value is then inserted into the event-trees that contain such event.

However, from a simulation point of view we are not seeking *if* an action is performed but rather *when* such action is performed. Thus, we need a probability distribution function that defines the probability that such action will occur as function of time.

Table 5-1: SPAR-H model values for the five human interventions

Intervention	Stress/stressors	Complexity
Manual ADS activation	high (100%)	moderately (34%), nominal (66%)
Firewater injection	high (100%)	moderately (10%), high (90%)
Extended ECCS operation	extreme (10%) high (90%)	high (100%)
Increase CST capacity	high (100%)	moderately (100%)
Containment (PSP) venting	high (100%)	moderately (100%)

Table 5-2: Correspondenace table between complexity and stree/stressor level and time values

Complexity	Mean, mu [min]	Stress/stressors	Standard Deviation, sigma [min]
High	45	Extreme	30
Moderate	15	High	15
Nominal	5	Nominal	5

Table 5-3: Values for mu and sigma for the five human interventions listed in Table 5.1 using the correspondance values shown in Table 5-2

Intervention	*Mean, mu [min]*	*Standard Deviation, sigma [min]*
Manual ADS activation	*8.4*	*15*
Firewater injection	*42*	*15*
Extended ECCS operation	*45*	*16.5*
Increase CST capacity	*15*	*15*
Containment (PSP) venting	*15*	*15*

5.3.3 Clad Failure Temperature

Uncertainty in failure temperature for the clad is characterized by a triangular distribution having:

- Lower limit = 1800 F (982 C): PRA success criterion
- Upper limit = 2600 F (1427 C): Urbanic-Heidrick transition temperature
- Mode = 2200 F (1204 C): 10 CFR regulatory limit

5.3.4 HPCI/RCIC Failure Time

Initially, HPCI and RCIC were modeled to fail at any time between 0 and 8 hours into the simulation, but it was found that sampling them to shut off before ten minutes into the simulation would cause the simulation to crash extremely regularly. With that in mind, ten minutes was imposed as a lower bound on the sampling for the failure time of both HPCI and of RCIC.

5.3.5 Containment Failure Pressure

For the containment failure pressure distribution we used NUREG/CR-6706 [8] as main reference. This document reports a detailed analysis regarding containment pressure limits for BWR Mark I systems. The analysis takes into account aging of the containment and, in particular, corrosion at waterline in the PSP. One case will be considered: 50% corrosion at the waterline in suppression pool. For this particular case, NUREG/CR-6706 reports the following as predicted failure pressure values

- Lower bound = 74 psi (0.510 MPa)
- Upper bound = 134 psi (0.924 MPa)
- Best estimate = 114 psi (0.786 MPa)

These three values have been used to characterize a triangular distribution (similarly to what has been done for the clad failure temperature in Section 5.3.3): lower limit = 74 psi, mode = 114 psi and upper limit = 134 psi.

5.3.6 SRV stuck open

SRVs stuck open event is an on-demand failure. In this report we follow the PRA model structure in which 1 or 2 SRVs may fail stuck open. The value for such failure on demand is: 3.7×10^{-3} per demand.

5.3.7 Summary of Stochastic Parameters

A summary of the stochastic parameters modeled in our analysis is shown in Tables 5.4 and 5.5.

Table 5-4. Component failure parameters and their associated distribution.

	Parameter	*Distribution*
1	*Failure time of DGs*	*Exponential*
2	*Recovery time of DGs*	*Weibull*
3	*Battery life*	*Uniform*
4	*SRVs stuck open*	*On demand*
5	*Offsite AC power recovery*	*Lognormal*
6	*Clad Fail temperature*	*Triangular*
7	*Containment failure pressure*	*Triangular*
8	*Seal LOCA time*	*Uniform*
9	*Seal LOCA flow rate*	*Lognormal*
10	*HPCI fails to run*	*Exponential*
11	*RCIC fails to run*	*Exponential*
12	*Reactor power*	*Uniform*

Table 5-5: List of human operator actions

	Parameter	*Distribution*
1	*Manual ADS activation*	*Lognormal*
2	*Firewater injection*	*Lognormal*
3	*Extended ECCS operation*	*Lognormal*
4	*Increase CST capacity*	*Lognormal*
5	*Containment (SP) venting*	*Lognormal*

In addition, as part of separate analysis we also considered the impact of uncertainties related to initial water level and temperature of the PSP. These two parameters are, however, not considered in the overall sensitivity analysis.

5.4 Stochastic Analysis

The stochastic analysis for the BWR SBO test case has been performed using the code RAVEN that is currently under development at INL. Originally, RAVEN was designed to control the code RELAP-7 but its capabilities have been extended to include also stochastic analysis methodologies (also known as dynamic PRA) such as Monte-Carlo and Dynamic Event Tree algorithms.

In addition, recently RAVEN has been coupled to RELAP-5. Such coupling allows performing multiple RELAP-5 runs (Monte-Carlo) but it is not able to control the RELAP-5 simulation run while it is running (a feature available when coupled to RELAP-7). Consequently, RELAP-5 control logic has been implemented within the RELAP-5 input file.

The stochastic analysis (i.e., Monte-Carlo) is performed through the following steps (see Figure 5-8):

1. Probability distributions for the considered stochastic parameters are obtained from the PRA

2. A link between the considered stochastic parameters and the parameters coded in the RELAP-5 input file is established by RAVEN

3. A set of *N* RELAP-5 input files are generated and values for the considered stochastic parameters are randomly sampled from their own distributions and plugged within the input files

4. Through the use of high performance computing capabilities of INL, all RELAP-5 runs are distributed on all available nodes and cores

5. When all simulation runs are completed, RAVEN generated an output file (in .csv format) for each simulation for the original RELAP-5 output file

6. All .csv files generated can now be analyzed using state-of-the-art data analysis algorithms which include:

    a. Classification based algorithms such as support vector machines or Gaussian process models

    b. Multi-dimensional data visualization tools

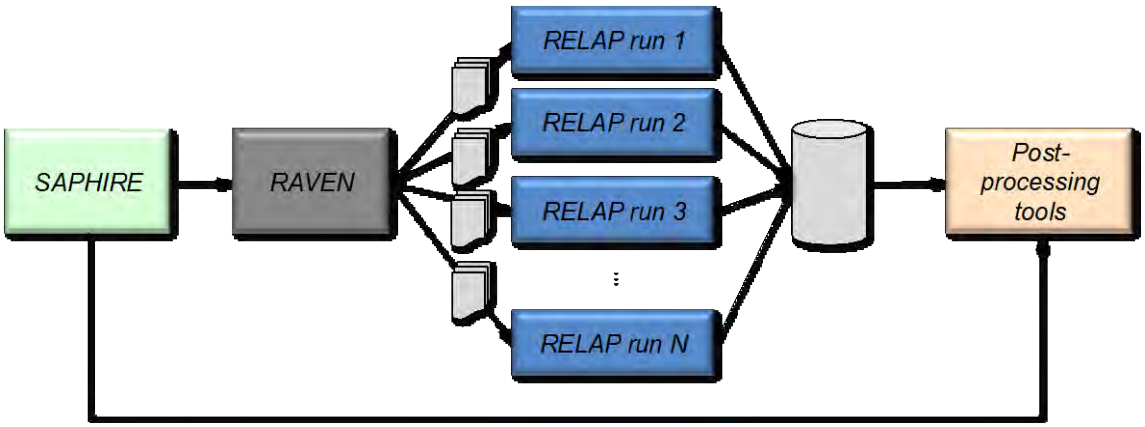

Figure 5-8: Scheme of the Stochastic Analysis using RELAP-5 coupled with RAVEN

6. SAFETY MARGINS ANALYSIS

In the past few years, the nuclear power industry has considered the following changes:

- Life extension: extended life from 40 years to 60 and even 80 years
- Power uprates: increase of the steady-state thermal power generated by the core (up to a 20% increase)

The scope of this report is to evaluate the impact of power uprates on SBO accident scenarios. From a safety point of view, a LOOP+SBO accident scenario follows these steps (see Figure 6-1):

1. At time t = 0, LOOP occurs

2. At time t = T_{SBO}, DG are lost: from this point the NPP staff try to recover AC power (DG or off-site power grid)

3. At time T_{ADS}, the heat capacity limits are reached and ADS is activated. Since core cooling is not available, core temperature cannot be controlled. Only available options are:

    a. Recover AC power

    b. Inject fire-water into the RPV

A higher value (from the original nominal level) of thermal power in the core causes the following:

1. Faster heating of the PSP and, thus, a reduction of the time interval between ADS activation time and loss of DG time, i.e., T_{ADS}-T_{SBO}

2. A faster heat-up after ADS activation; thus leading to less time available to the plant staff to align the firewater

In summary, a power uprate reduces:

- Time available to the plant staff to recover AC power
- Time available to the plant staff to align FW

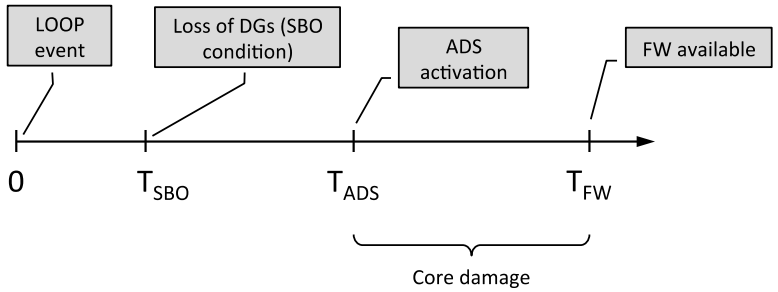

Figure 6-1: Typical SBO sequence of events

In this section we evaluate and quantify such time reductions.

6.1 PSP heat capacity limits

This section shows some of the preliminary results regarding the effect of power uprates on SBO accident scenario.

6.1.1 PSP temperature versus reactor power levels

We performed an initial evaluation of the impact of a power uprate by observing the PSP temperature increase rate as function of the thermal power generated by the core (see left image of Figure 6-2). In particular, we looked at the time to reach the PSP temperature limits for different values of core power (ranging from 100% to 120%). These results are shown on the right image of Figure 6-2. For this set of simulations we fixed T_{SBO} = 1h and we, thus, measured T_{ADS}-T_{SBO} (see Figure 6-1).

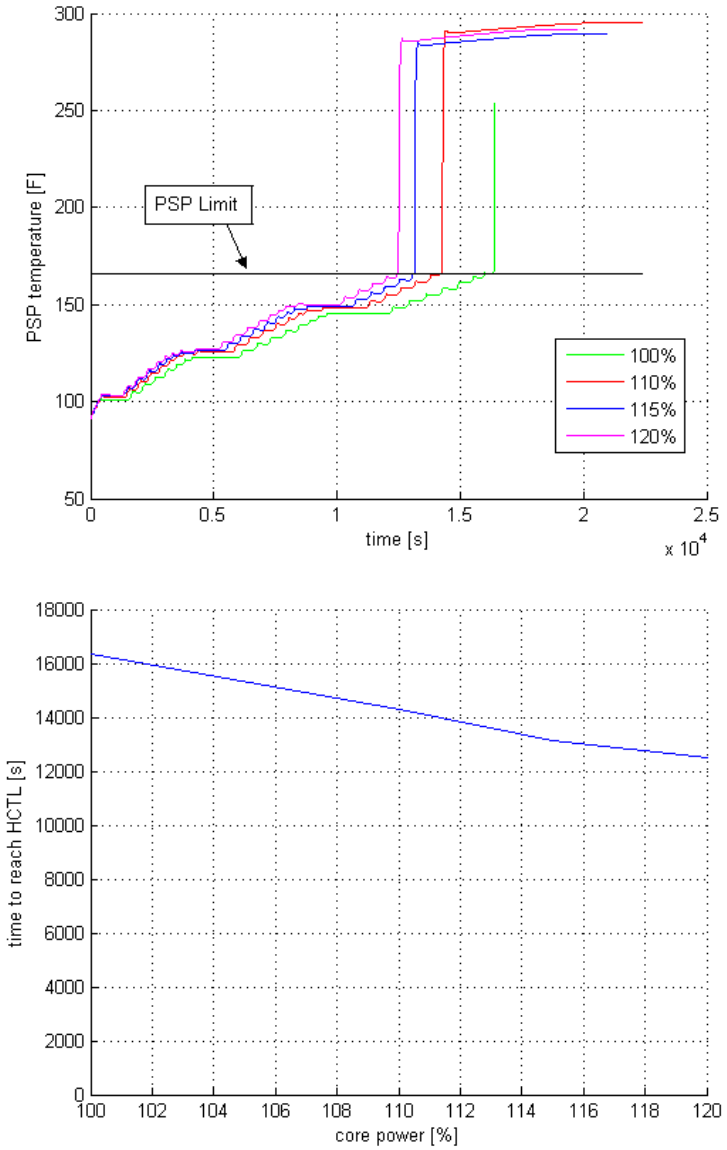

Figure 6-2: Impact of reactor power uprate on time to reach PSP heat capacity limits HCTL

As expected, by increasing the core power the time to reach the PSP heat capacity limits decrease. In the left graph, the PSP temperature can be seen increasing in small steps as the SRVs open and close, and remaining relatively flat for a longer period of time whenever HPCI/RCIC activates and it is unnecessary to open the SRVs for a longer period of time. The sudden large increase in PSP temperature in each simulation is when the PSP heat capacity limit is reached and the ADS activates, dumping a large amount of steam from the RPV into the PSP. Note that (Figure 6-2 right), if reactor power is increased to 110% and 120%, the time to reach core HCTL limits decrease from 4.5 h (16300 s) to 3.9 h (14100 s) and 3.5 h (12400 s), respectively.

6.1.2 Impact of DG failure time

In the analysis for Section 6.1.1 we kept the T_{SBO} = 1h. Given the fact that decay heat power generated by the core after a successful shutdown drops exponentially, a late failure time of DGs allows the plant to remove a large fraction of the decay heat. So we expect that the time to reach PSP HCTL will increase when T_{SBO} increases. Analogously an increase in core power will negatively affect time to reach PSP HCTL.

In order to confirm and quantify such a prediction, we performed a set of simulations runs where we changed both reactor power (100%, 110% and 120%) and failure time of DGs (T_{SBO}). Results are summarized in Figure 6-3.

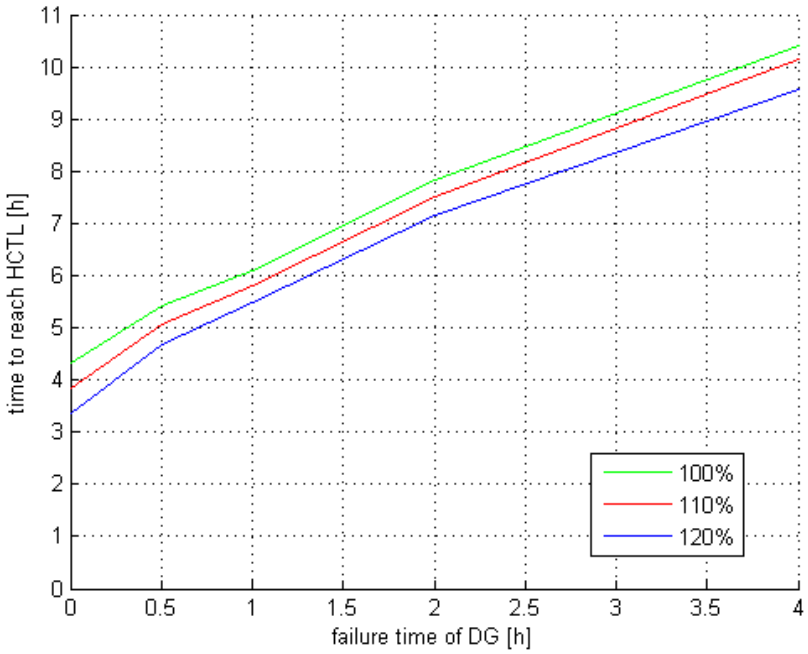

Figure 6-3: Time to reach PSP HCTL as function of DG failure time T_{SBO} and reactor power

Note that the "time to reach HCTL" data is actually T_{ADS}-T_{SBO} (see Figure 6.1).

As expected, being able to maintain AC powered core cooling for an extended period of time increases the time until the PSP Heat Capacity Limits are reached, and increasing the core power decreases the time until the PSP Heat Capacity Limits are reached. This is because the PSP has a limited amount of heat it can take in before the Heat Capacity Limits are reached. Delaying the SBO time lowers

the amount of core heat being produced at the time of SBO and lowers the rate at which heat is added to the PSP. Likewise, increasing core power increases the amount of core heat being produced when the SBO transient starts, and heat is added to the PSP more quickly.

6.1.3 Impact of PSP initial conditions

As an additional analysis we also investigated how the PSP initial conditions (in terms of temperature and pressure) would affect the time to reach PSP HCTL. The driving idea was the following: in Sections 6.1.1 and 6.1.2, the power uprate (e.g., a higher nominal core power level) and T_{SBO} reduce the time to reach PSP HCTL. The question then is "it possible to compensate such reduction by increasing the heat capacity of the PSP?" The increase of the PSP heat capacity could occur by increasing the water volume or by keeping the PSP water cooler.

Note that these two parameters are considered fixed in the rest of report: PSP level at 15 ft and PSP temperature at 90 F.

Thus, we expect that by increasing the PSP heat capacity (i.e., higher water level or lower PSP initial temperature), the time to reach HCTL (i.e., T_{ADS}-T_{SBO}) increases. This is confirmed by the obtained results shown in Figure 6-4.

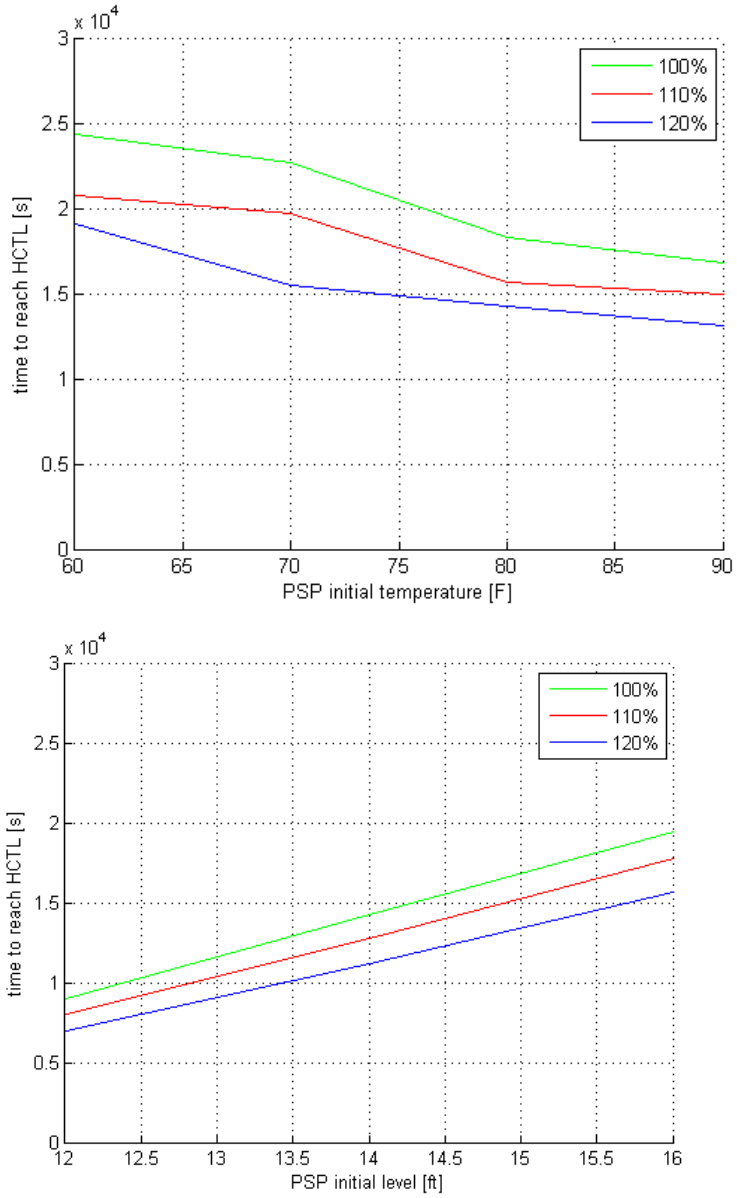

Figure 6-4: Time to reach PSP HCTL as function of PSP initial temperature (top), PSP initial level (bottom) and reactor power

Interestingly, in the time to reach HCTL versus PSP initial temperature graph, the data for 100% power and 110% power have very similar profiles, while 120% power has a different, but not unreasonable profile. At many points in testing the model and processing data, it seemed that there were many "break points" in the data where a slight adjustment in a given parameter would result in a much greater change in results than expected. These seem to be due to the cyclic nature of the SRVs and HPCI/RCIC systems, and due to the discrete nature of the way the control logic was implemented – in general, systems are binary and either on or off, with little to no middle ground. A theoretical example of one of these break points: if the PSP is 0.1 degrees Fahrenheit below the PSP heat capacity limit when the SRVs close at the pressure high set point, the ADS will activate several minutes later than if the PSP had an initial temperature 0.1 degrees Fahrenheit higher. This effect is even more pronounced when at the

points in time where RCIC activates, as the sudden injection of large amounts of cold water prevents the need to open the SRVs for nearly half an hour, resulting in large "break points" in the data where a minor decrease in the PSP initial temperature, or change in a given sampled parameter, can have a greatly disproportionate impact on the course of events in the SBO simulation.

In the PSP initial temperature testing, it appears that a break point in the data lay between 70 and 80 degrees Fahrenheit for both 100% and 110% power, while it was between 60 and 70 degrees Fahrenheit for 120% power, explaining the differing profile. In the time to reach HCTL vs. PSP initial level graph, there are no such discrepancies – presumably any such break points in the data do not straddle any of the sampled conditions for the PSP.

6.2 Impact of battery failure time and firewater availability time

Our second set of experiments focused on the determination on the "limit surfaces", i.e. boundaries in the input space that separates failure from success. As a first step we focused on considering a 2-dimensional input space: FW availability time (measured after ADS activation, i.e. T_{FW}-T_{ADS}) and battery life. By randomly changing these two parameters we observe the outcome of each simulation (failure or success) and, by using a Support Vector Machines (SVM) [9, 10] based classifier, we determine the limit surface.

Obviously, we expect that success will occur when FW is available shortly after ADS activation and for long values of battery life. Recall that, in fact, in order to activate ADS, DC power provided by batteries needs to be available.

Results are shown in Figure 6-5 for three different values of power: 100%, 110% and 120%. Success in these scenarios was considered to be recovery of AC power (which was sampled as being impossible) or alignment of the firewater injection lines. As expected, a longer battery life and a shorter firewater injection alignment time lead to success, while a short battery life and long firewater alignment time leads to failures. The slope at the left end of the success space represents situations where battery power cuts out, the SRVs de-energize and close, and the RPV re-pressurizes just before the firewater can be aligned.

Interestingly, in order to guarantee success, a minimum battery life as needed, and a higher core power allowed for the core to remain protected with a shorter battery life where a lower power core would have failed. This is due to the fact that the simulation did not account for the possibility of a manual ADS activation, and required that the heat curves for the plant be exceeded before ADS activation. In a higher power simulation, the heat curves are exceeded more quickly, so the plant blows down sooner and less battery life is needed. The tradeoff to this is that the firewater must be aligned more quickly in the higher power simulations than the lower power simulations, which is not a worthwhile tradeoff in a real situation, as the ADS can be activated early in a real situation if the firewater injection is ready before the heat curves are exceeded. Consequently, to represent this situation in a more realistic fashion, a future analysis should include a more detailed probabilistic human model that would include the possibility of FW alignment operation start time before the actual ADS activation (e.g., an alternative emergency operating procedure).

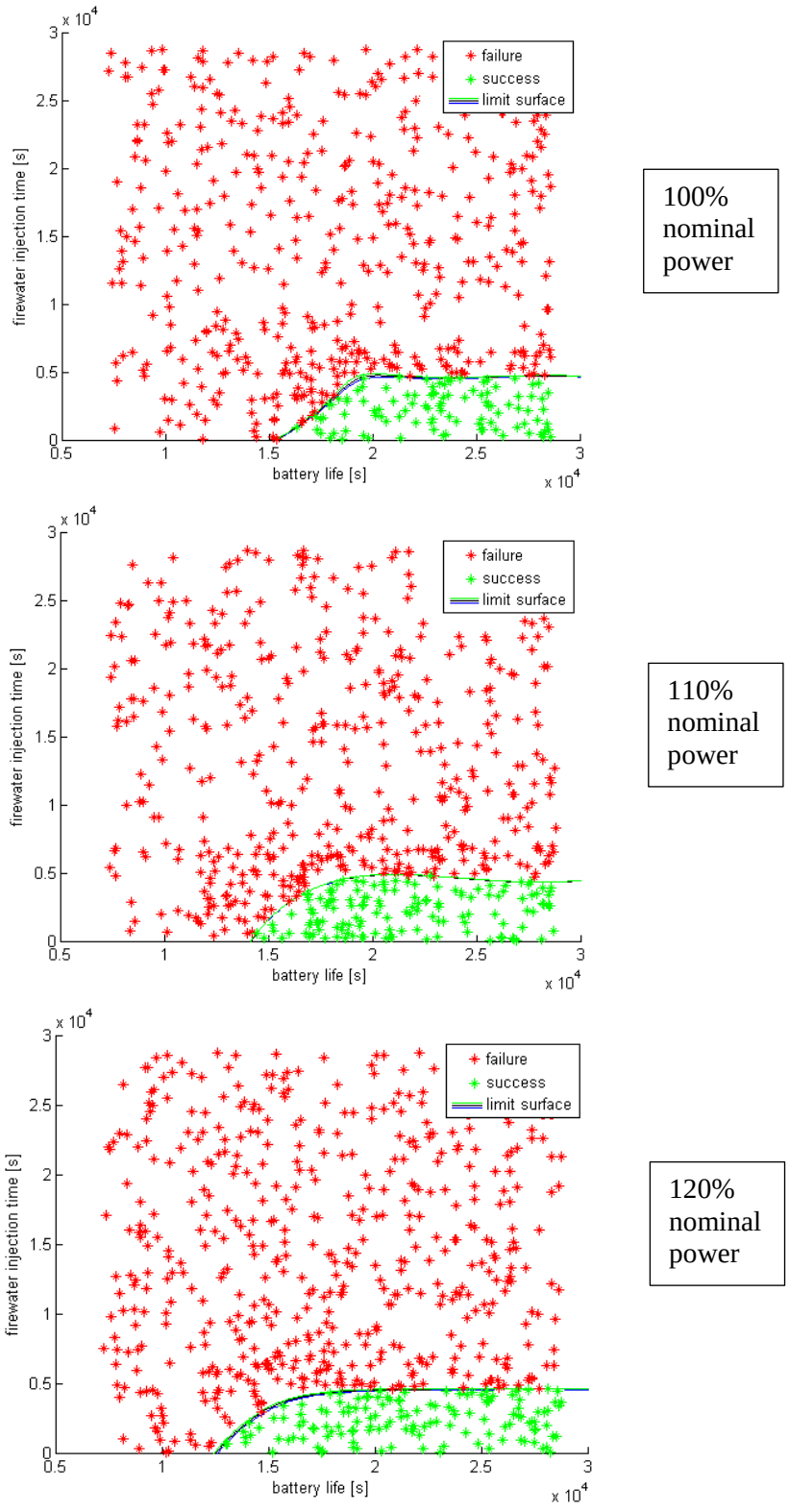

Figure 6-5: FW availability time vs. Battery life: limit surface for 100% (top), 110% (middle) and 120% (bottom) power

6.3 Firewater injection and AC power recovery timing

Similarly to what it has been done in Section 6.2, we determine the limit surface for a different 2-dimensional input space: DG failure time vs. AC power recovery time (either DG recovery or off-site power recovery). Thus, we sample these two parameters uniformly over the space and we observed the final outcome of the simulation (success or failure). Using the same SVM [8,9] classifier we thus determined the limit surface.

For this case, we expect that failure occurs for early DG failure time (i.e., early T_{SBO}) and late AC recovery time. In other words we expect failure for long time interval between AC power lost and AC power recovery events.

Limit surfaces are shown in Figure 6-6 for three different values of power levels: 100% (top), 110% (middle) and 120% (bottom). As expected, failures occur when AC power is lost for a long time and for early failure of DG.

Note that if reactor power increases, time to reach PSP HCTL limits and time to reach core damage decreases. Thus, the time that the plant staff has to recover AC power shrinks.

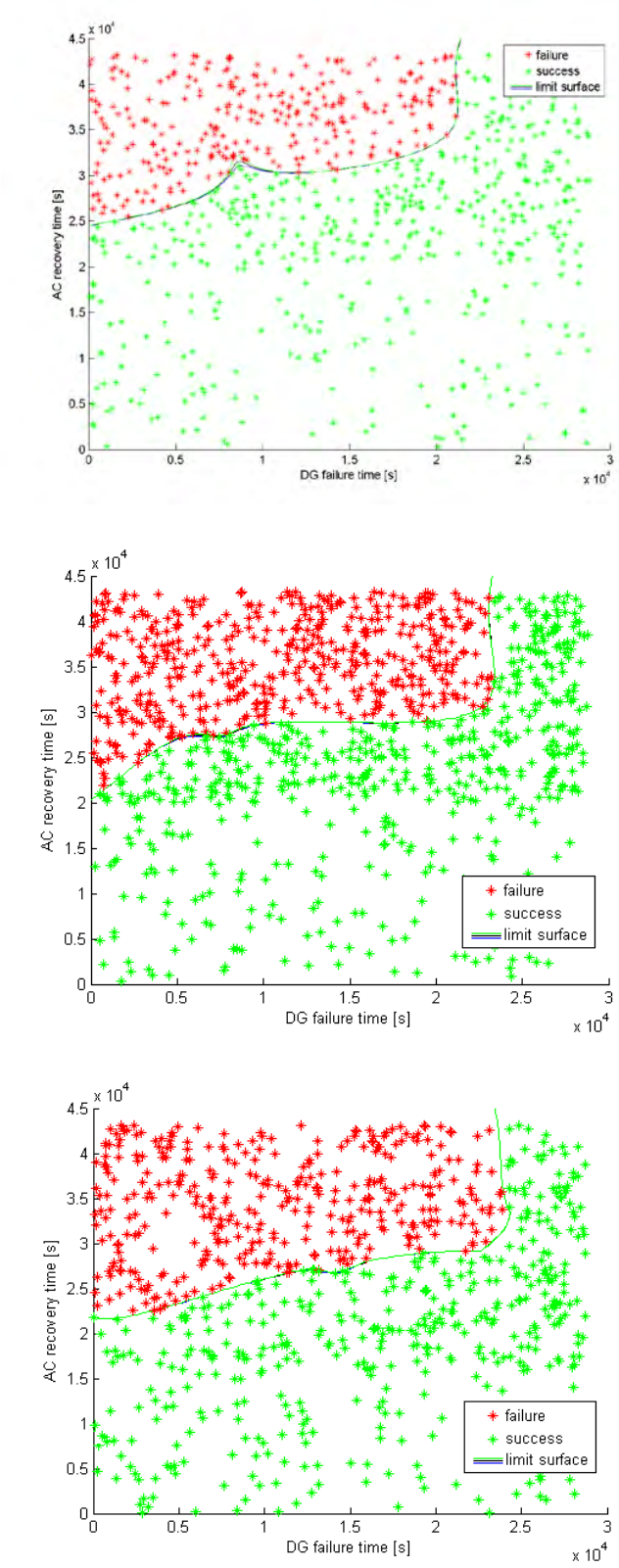

Figure 6-6: AC recovery time vs. DG failure time: limit surface for 100% (top), 110% (middle) and 120% (bottom) power

6.3.1 Impact of DGs failure time on time to ADS activation and time to core damage

This section aims to summarize the effect of power uprates on the most relevant timing of events during an SBO accident scenario. We consider three timing of events (see Figure 6-7):

1. DG failure time, i.e. T_{SBO}
2. Time to activate ADS, i.e., T_{ADS}-T_{SBO}
3. Time to reach core damage (measured from T_{SBO}), i.e., T_{CD}-T_{SBO}

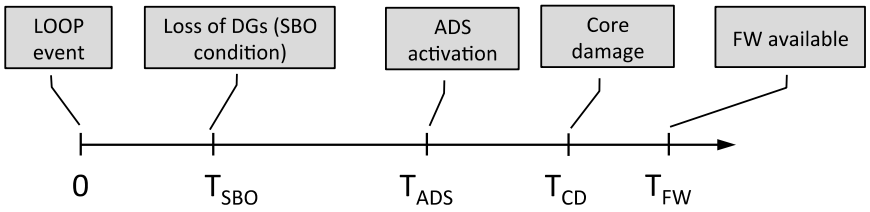

Figure 6-7: Sequencing and timing of events for a SBO accident scenario

Results are shown in Figures 6-8, 6-9 and 6-10. Note the following:

- To generate Figures 6-8, 6-9 and 6-10 we selected, for each power level (100%, 110% and 120%), a set of values for T_{SBO}. We then run a set of simulation runs and identified that time at which the reactor operators need to activate the ADS. Compared to what is presented in Figure 6-2, this analysis considered not just PSP temperature as indication to trigger ADS activation but all the curves shown in Figure 3-4. In addition, AC power is not recovered and FW is never available.

- Figure 6-8 shows T_{SBO} (x axis) vs. T_{ADS}-T_{SBO} (y axis). By increasing T_{SBO}, we expect that the reactor operators are required to activate ADS much later. Again, a reactor power increase negatively affects ADS activation time.

- Figure 6-9 shows T_{SBO} (x axis) vs. T_{CD}-T_{SBO} (y axis). Similarly to Figure 6-9, if AC power is available for a long time, the PSP HCTL limits are reached further in time. This allows to reach core damage much later.

- This set of tests was much more extensively covered than the ones shown in the previous sections due to the chaotic nature of the data. Initial sampling was done with the EDGs failing at 0 seconds, 3600 seconds, 7200 seconds, and 14400 seconds. After this proved to be insufficient, more simulations were run with the EDG failure time set to be every 720 seconds, up to 14400 seconds, producing the data shown in Figures 6-8, 6.9 and 6-10.

- The data in Figure 6-10 was expected to be rather jagged, for two reasons. It has the same level of "signal noise" as Figures 6-8 and 6-9, but is on a smaller absolute scale than either Figures 6-8 and 6-9. Additionally, the cyclical nature of the SRVs and HPCI/RCIC activation means that beyond any signal noise, the data is expected to fluctuate a certain amount – if ADS activation happens when the core level is low, just above the HPCI/RCIC low level set point, the core will have a lower water level than it would if the core level had been very high when ADS activation occurred. The time between ADS activation and core

damage depends not only on the core power and the EDG failure time, but also on much more difficult to control and predict variables like the core level and pressure at the time of ADS activation.

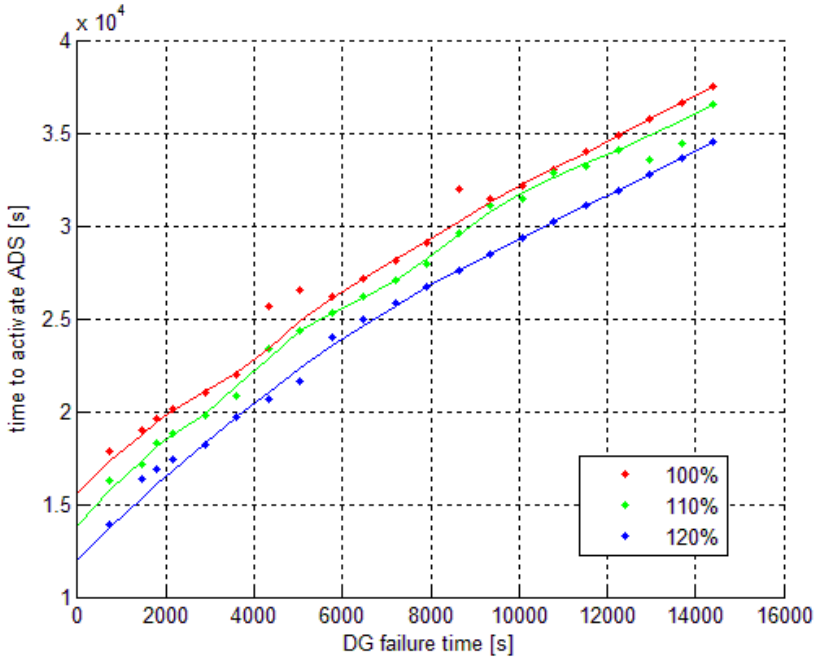

Figure 6-8: Time to activate ADS vs. DG failure time, curves for 100% 110% and 120% power

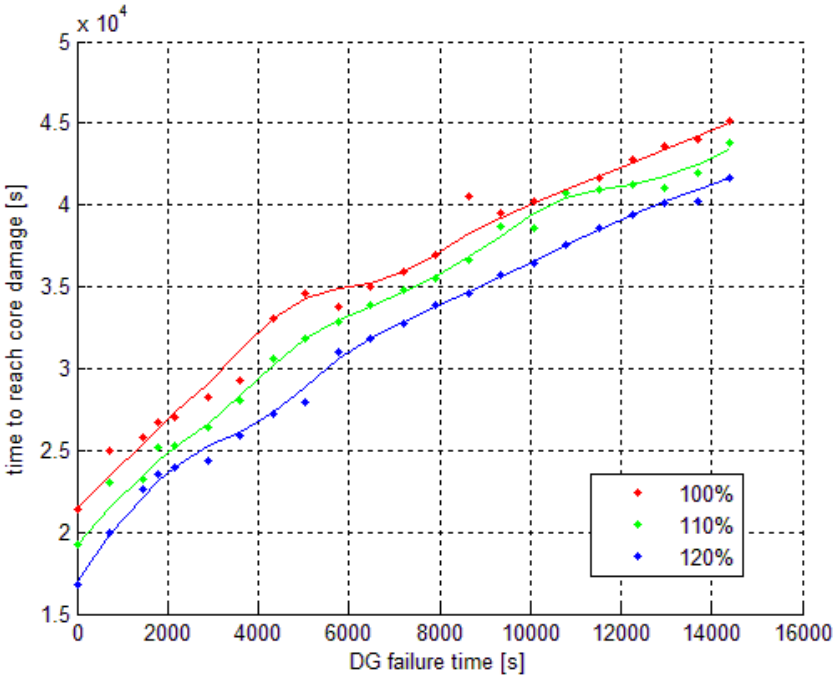

Figure 6-9: Time to reach core damage vs. DG failure time, curves for 100% 110% and 120% power

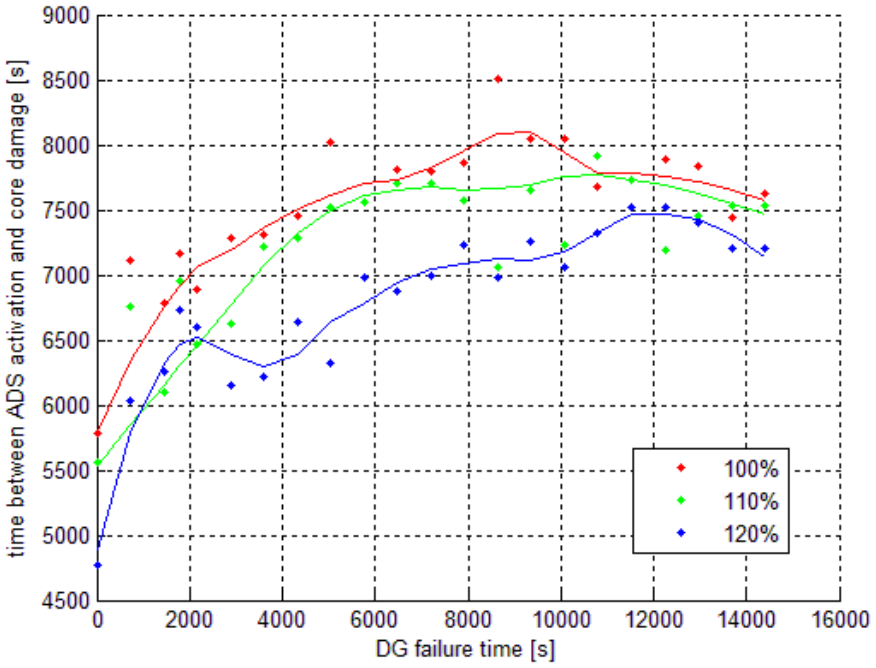

Figure 6-10: Time between ADS activation and time to reach core damage vs. DG failure time, curves for 100% 110% and 120% power

6.3.2 Impact of RCIC Failure time on time to ADS Activation

This section discusses the impact of failure of HP water injection (both RCIC and HPCI). We chose a set of failure time values for both RCIC and HPCI and, for each simulation run, we measured the time required by the reactor operators to activate ADS. We kept T_{SBO} constant at 1 h and high-pressure injection failure time is measured from T_{SBO}.

When cooling is no longer available, we expect that the operators will be required to activate ADS sooner. However, due to intrinsic cycling of RCIC/HPCI we do not expect a linear smooth behavior. A failure in the HP injection system will, in fact affect ADS activation only when HP injection is needed.

A summary of the results is presented in Figure 6-11 for three different power levels (100%, 110% and 120%).

Figure 6-11 nicely demonstrates the cyclical nature of the model and of the break points in the data previously discussed. This is explained in Figure 6-12, which is simply RPV pressure data from a run of the simulation where RCIC was set to never fail and core power was set to 100%. When the pressure is oscillating relatively quickly, the SRVs alone are maintaining the pressure, and RCIC is not in use. When the pressure dips slowly, RCIC is engaged and raising the core water level to stave off core damage. The flat regions in the data in Figure 6-11 are caused when the RCIC failure time is during a period of inactivity – in Figure 6-12, it can be seen that RCIC is inactive from 6400 seconds to 9400 seconds – any tested RCIC failure time in this period will not impact the time to ADS activation. The data in Figure 6-11 cuts off at the lower end at ten minutes, because setting RCIC to fail before ten minutes caused the

simulation to crash and fail. Unexpectedly, there are certain periods of time where a higher core power does slightly better than a lower core power – this is because the higher core power causes RCIC to turn on sooner and inject cold water into the core just before it fails, and the later activation time in the lower core power means that RCIC does not have the chance to turn on and refill the core.

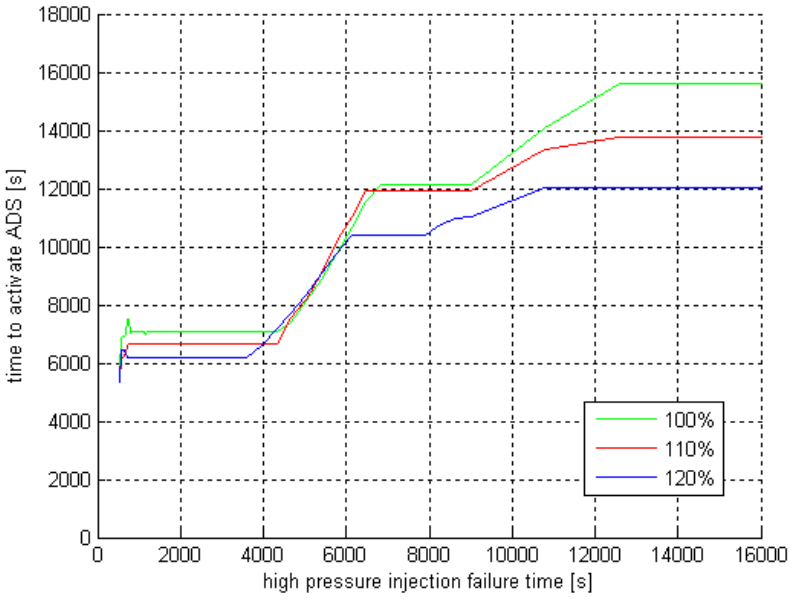

Figure 6-11: Dependence between time to activate and failure time of high-pressure injection systems (RCIC and HPCI) for three different power levels (100%, 110% and 120%)

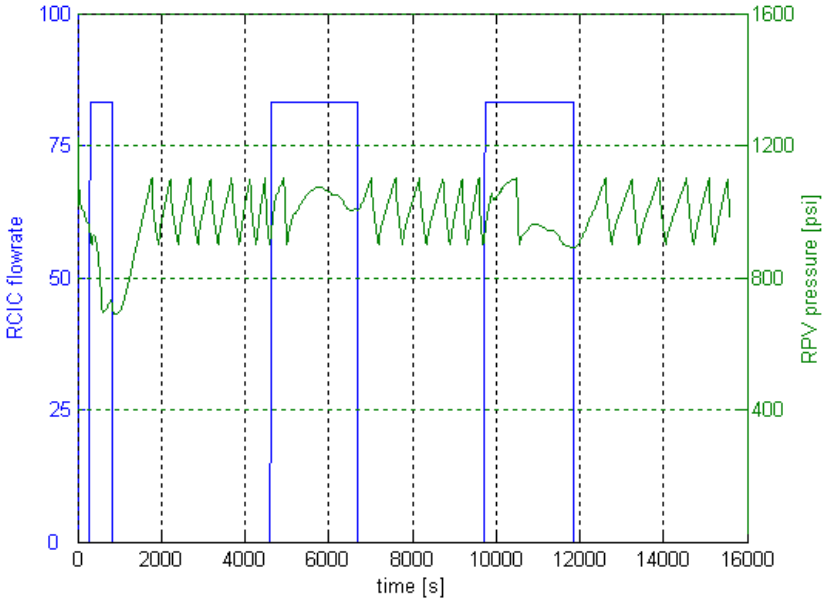

Figure 6-12: Cycling of SRVs (green line) and RCIC (blue line) as function of time for a SBO accident scenario for a power level of 110%

6.4 Impact of Seal LOCA

Due to the fact that the pump seal LOCA model instability was drastically increasing the probability of simulation crash, we performed a separate analysis to evaluate the impact of this event on the SBO accident scenario. In the event of a pump seal LOCA, the water leakage from the pump seal heat the drywell, i.e., drywell temperature and pressure increase. Such temperature/pressure increase triggers the activation of the ADS when temperature of values and temperature in the drywell overcome the DW/T-2 curve line shown in Figure 3-4.

The drywell temperature/pressure rise rate is independent of when the seal LOCA occurs but it rather depends on the water flow rate leaking from the pump seal. Thus, we investigated the dependence between seal LOCA flow rate and time to activate ADS. We selected several values of SEAL flow rate values and measured, for each simulation runs, the time at which T/H conditions in the drywell exceed the DW/T-2 curve line shown in Figure 3-4.

Results are shown in Figure 6-13: naturally, large seal LOCA flow rate will cause a steep rise of the drywell T/H conditions and, hence, ADS will be activated shortly after seal LOCA occurs. Analogously, for very small leakage rate ADS might not even need to be activated.

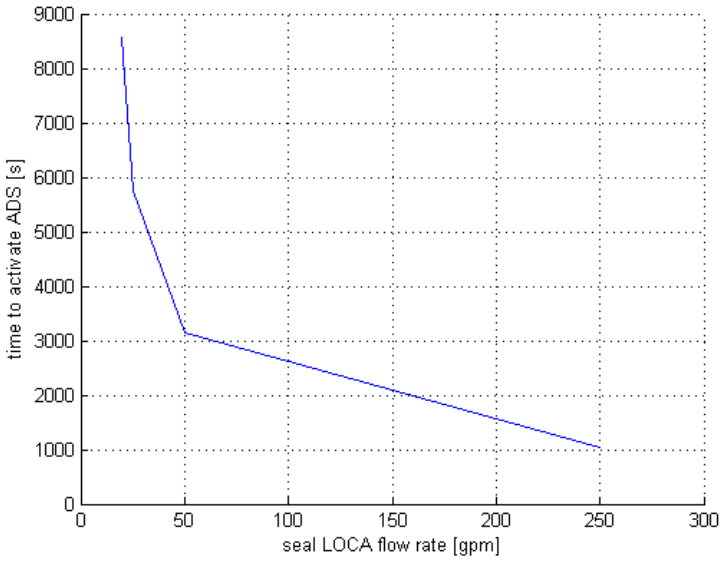

Figure 6-13: Dependence between seal LOCA flow rate and time to activate ADS (i.e., when T/H conditions in the drywell exceed the DW/T-2 curve line shown in Figure 3-4)

As one would expect, increasing the flow on a Pump Seal LOCA significantly decreased the amount of time it takes for the Drywell to reach its temperature limits and trigger the ADS.

6.5 Impact of clad failure temperature on time to core damage

From a safety point of view, uncertainties associated with the clad failure temperature are particularly relevant as they affect the time to reach core damage. In order to quantify such dependence, we fixed T_{SBO} at 1 h, power at 100% and we set several values for clad failure temperature. Then, for each simulation we measured the time to reach core damage, i.e., when maximum clad temperature is equal or greater than clad fail temperature. Results are shown in Figure 6-14.

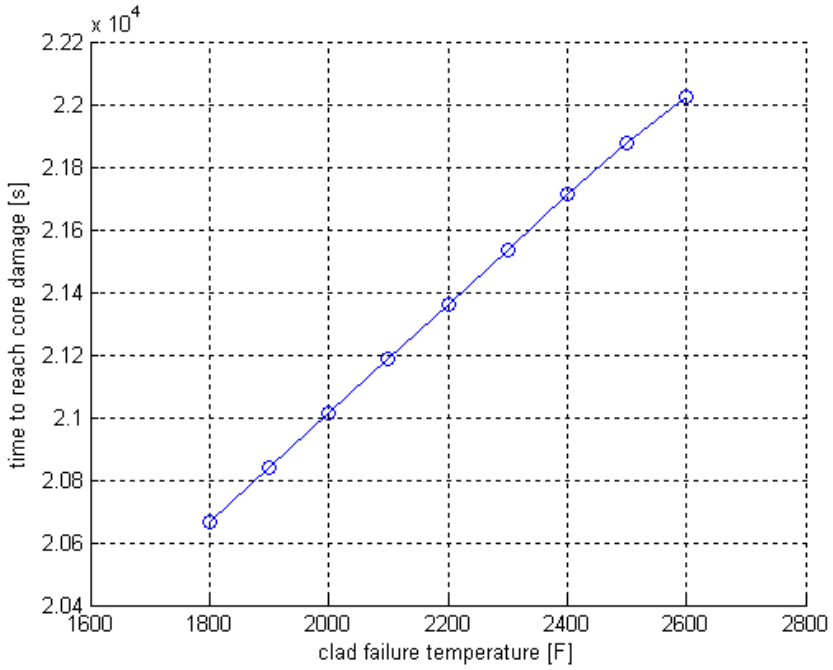

Figure 6-14: Dependence between clad failure temperature and time reach core damaged (i.e., T_{CD}-T_{SBO} as shown in Figure 6-7)

As expected, fuel cladding melting point appears to have a strong linear relationship with the time to melt. In theory, a high enough melting point would delay core damage long enough that the exponential nature of the decay heat would degrade the linearity of the relationship between the melting point and time to core damage, but for a change from ~20700 to ~22000 seconds, the change in decay heat is insignificant, and the relationship remains linear.

7. UNCERTAINTY ANALYSIS

In order to evaluate the impact of the uncertain parameters listed in Section 3 on the simulation outcome we performed an extensive Monte-Carlo analysis that consisted of generating 20,000 Monte-Carlo runs. We performed our analysis using the High Performance Computational capabilities of INL and, in particular, we employed the Fission super-computer[5]. Using 8 nodes and a total of 256 CPUs (32 CPUs/node), we were able to run 20,000 cases in about 3 days.

From these 20,000 cases we identified the following:

- Four simulation runs crashed (possible caused in the PSP right after ADS activation); thus, the effective number of runs is 19,996
- Clad temperature limits were always reached before PSP pressure limits; thus, simulations leading to containment failure were never observed
- As a consequence of the fact that PSP pressure limits have never been reach, the stochastic parameter "Containment venting" was irrelevant to the analysis
- CST original capacity has never been passed in every simulation; hence, the stochastic parameter "Increase CST capacity" was irrelevant to the analysis
- Due to RAVEN-RELAP-5 interface issues, battery life and extended ECCS operation have been merged into a single parameter "Total battery life"
- Due to seal LOCA model instability, the two stochastic parameters related to this event (seal LOCA time and flowrate) were not considered

We apply clustering algorithms based on Morse-Smale complex [11] on the dataset obtained from a RAVEN for the BWR LOOP+SBO MC analysis (see Appendix C). From this simulation data set we extracted the value of the maximum temperature reached in the core.

We then model the maximum core temperature variable as a high-dimensional scalar function f in an n-dimensional space X (where n is the number of stochastic parameters). Each simulation corresponds to a data point in X. We partition the points in X based on their function values and gradient behavior with respect to the approximated Morse-Smale complex. That is, points belong to the same cluster if they have uniform gradient flow behavior.

We further obtain topological summary for each cluster and try to infer the correlations between simulation parameters and system observations. Researchers in the field of clustering algorithms are

[5] Fission computer cluster data:
- 12,512 core Appro distributed memory system
- 391 computer nodes with four processor sockets per node
- four 8x2.4GHz AMD Opteron processor 6136
- 64 GB memory
- QDR InfiniBand, Fat Tree Topology over-subscribed 3.5:1
- Operating System: Red Hat Linux Enterprise Server 5.7
- LINPACK: 91.03 TFlops

interested in what combination of conditions (in the form of input simulation parameters) can cause potential reactor failure (i.e. nuclear meltdown witnessed by maximum core temperature exceeding a threshold value). Furthermore, they are interested in the impact of increased reactor power on safety of the nuclear plant, in terms of time required for various recovery procedures.

An ensemble of 19,996 transient simulations has been generated, and among which 6,597 scenarios are considered system failures when the reactor reaches a maximum temperature before the end of simulation. The rest of the 13,399 scenarios are considered simulation completions/success. Each simulation includes information regarding the timing of various recovery attempts (e.g. cooling recovery, fire water, etc.), the reactor power level and the failure temperature threshold. There are 12 input parameters which encode uncertainty by sampling from a continuous range during simulation:

1. FailureTimeDG: Failure time of Diesel generators (DGs). This corresponds to the time of SBO event.
2. RecoveryTimeDG: Recovery time of DGs
3. OFFsitePowerRecoveryTime: Offsite AC power recovery time
4. SRV1stuckOpenTime: The time when 1 Safety Relief Valves (SRV) stuck open
5. SRV2stuckOpenTime: The time when 2 or more SRV stuck open
6. cladFailureTemperature: Uncertainty in failure temperature for the clad
7. HPCIFailToRunTime: The time when High Pressure Core Injection (HPCI) fails to run.
8. RCICFailToRunTime: The time when Reactor Core Isolation Cooling (RCIC) fails to run.
9. ReactorPower: Reactor power uprate. It is sampled between 1 = 100% and 1.2 = 120%,
10. ADSactivationTimeDelay: Manual Automatic Depressurization System (ADS) activation.
11. FirewaterTime: Firewater injection time
12. TotalBatteryLife: battery life + extended ECCS operation

All the above time-related parameters are measured from the time of the SBO event (in seconds), which is the FailureTimeDG. The output variable obtained from the transient simulation is maxCladTemp, which is the maximum clad temperature reached during the entire course of the simulation. Such a variable is less or equal to the failure temperature threshold (e.g cladFailureTemperature). In addition, an additional discrete variable outcome is given to classify success (outcome = -1) from failure (outcome = +1) scenarios.

7.1 Data Pre-Processing

Before analyze the data we performed a series of pre-processing procedures:

- **Data standardization:** The above data is pre-processed with a standardization process. Since different parameters may be measured on different scales and the range of values differ from each dimension, some parameters may dominate the results of the analysis. We

employ a data standardization process so that all dimensions are on the same scale. For values of each dimension, we subtract the mean and divide by the standard deviation. Although more robust approaches are available, the above technique is usually sufficient.

- **Number of dimensions reduction:** Upon further observations of the nature of the simulation dynamics, we further transform the data by reducing the number of dimensions Reduction process is carried out such that input stochastic parameters that have same impact on system dynamics are merged together. In particular, we introduce 3 new dimensions after eliminating 6 dimensions from the raw dataset:

  - ACPowerRecoveryTime: min {RecoveryTimeDG; OFFsitePowerRecoveryTime}.
  - SRVstuckopen: min {SRV1stuckopen; SRV2stuckopen}.
  - CoolingFailtoRunTime: max {HPCIFailToRunTime; RCICFailToRunTime}.

  Ultimately, the 9D case includes the following input variables: (1) FailureTimeDG; (2) ACPowerRecoveryTime; (3) SRVstuckOpenTime; (4) cladFailureTemperature; (5) CoolingFailtoRunTime; (6) ReactorPower; (7) ADSactivation-TimeDelay; (8) firewaterTime; (9) TotalBatteryLife. The output variable is the maxCladTemp (MT).

7.2 Case 9D-MT-all-3C

The first data-set we consider, called "9D-MT-all-3C," consists of:

- 19,996 data points
- 9 dimensions, i.e., 9 input variable
- Output variable is maximum clad temperature

Using the HDViz software [12, 13] (see Appendix C for details) and the from 9D-MT-all-3C data-set, we were able to obtain 3 "crystals/clusters[6]" as shown in Figure 7-1. Topological structure of the Clad max temperature as a 9-dimensional surface was characterized by a single local minima and 3 local maxima as indicated in These types of insights are important as we investigate risk-informed margins management approaches. Having an understanding of what is (or is not) important from these complex, multidimensional spaces is vital in order to focus the engineering portion (i.e., the proposed strategies) of risk management.

Table 7-1. This means that, from a local minima of *f* (no core damage), it is possible to reach three local maxima (high clad temperature) by following three different paths. Each of these paths is determined by changing the input stochastic parameter values.

Figure 7-2 show the projection of the three crystals for each dimension including regression curve: the x-axis corresponds to output variable (maximum clad temperature) while the y-axis corresponds to input variable. In addition, Figure 7-3 shows, for each crystal, the histogram distribution of a set of timing of events.

[6] Crystals/clusters are topological structures that connect local minima to local maxima of *f*. Each crystal/cluster contains a specific set of data points

From Figure 7-2 and Figure 7-3, and by looking at the regression curve obtained, we can see the following:

- A high value of clad temperature is reached, for all three crystals, for a late AC recovery time. As expected a late AC recovery time is a necessary condition to reach core damage
- The same conclusions can be drawn for FW injection time, a late FW injection time guarantee as well core damage
- Failure time of DGs differentiates the three crystals, i.e., a late DG failure time is not sufficed to guarantee system success. In fact, by looking at the green crystal regression curve, a late failure time of DGs coupled with early SRV stuck-open event and an early failure of the high-pressure injection system (both RCIC and HPCI) leads to core damage
- By looking at the regression curve of the purple crystal, core damage condition was reached for an early DGs failure time early failure the high-pressure injection system (both RCIC and HPCI)

These types of insights are important as we investigate risk-informed margins management approaches. Having an understanding of what is (or is not) important from these complex, multidimensional spaces is vital in order to focus the engineering portion (i.e., the proposed strategies) of risk management.

Table 7-1: Minima and maxima of the crystals of Figure 7-1

Crystal color (see Figure 7-1)	*Min*	*Max*
Red	*1008.80*	*2600.09*
Green	*1008.80*	*2597.20*
Blue	*1008.80*	*2534.16*

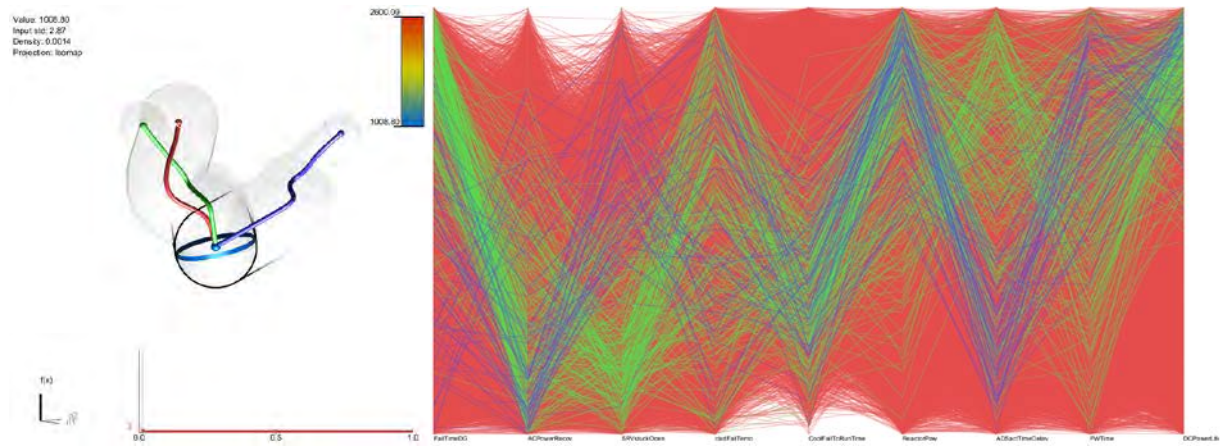

Figure 7-1: 9D-MT-all-3C: topological summary (left) and parallel coordinate plots for all three clusters (right)

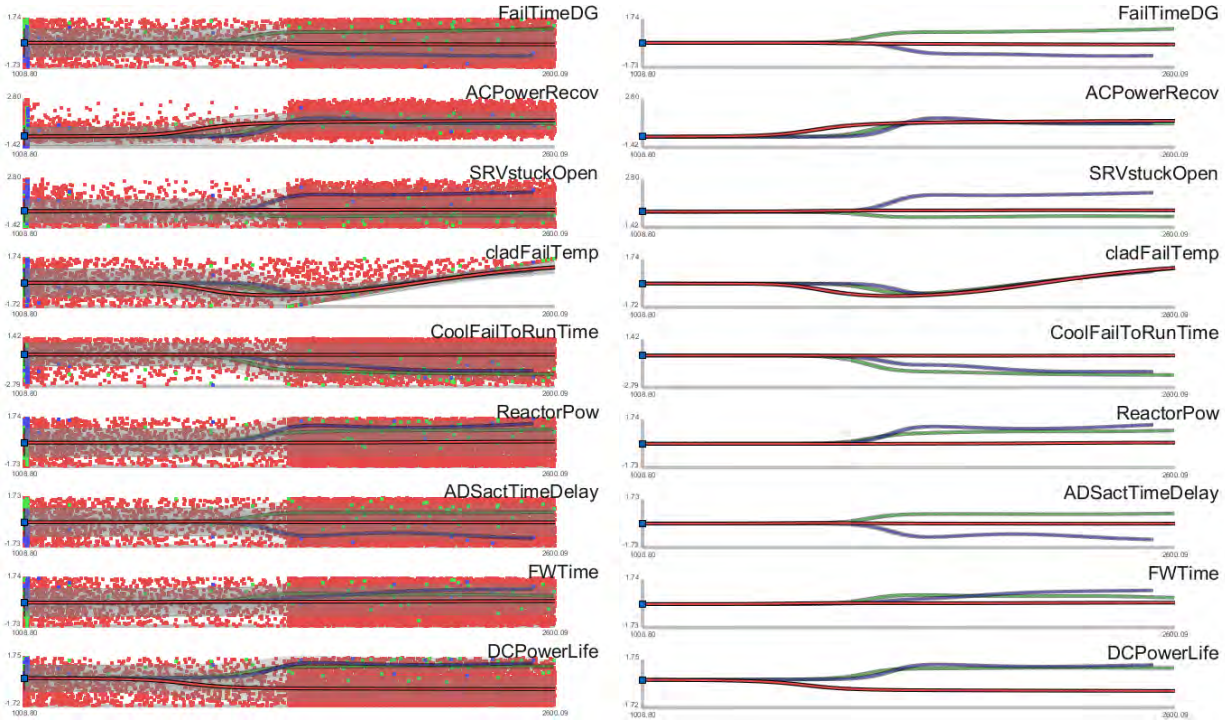

Figure 7-2: 9D-MT-all-3C: inverse coordinate plots with (left) and without (right) points projection

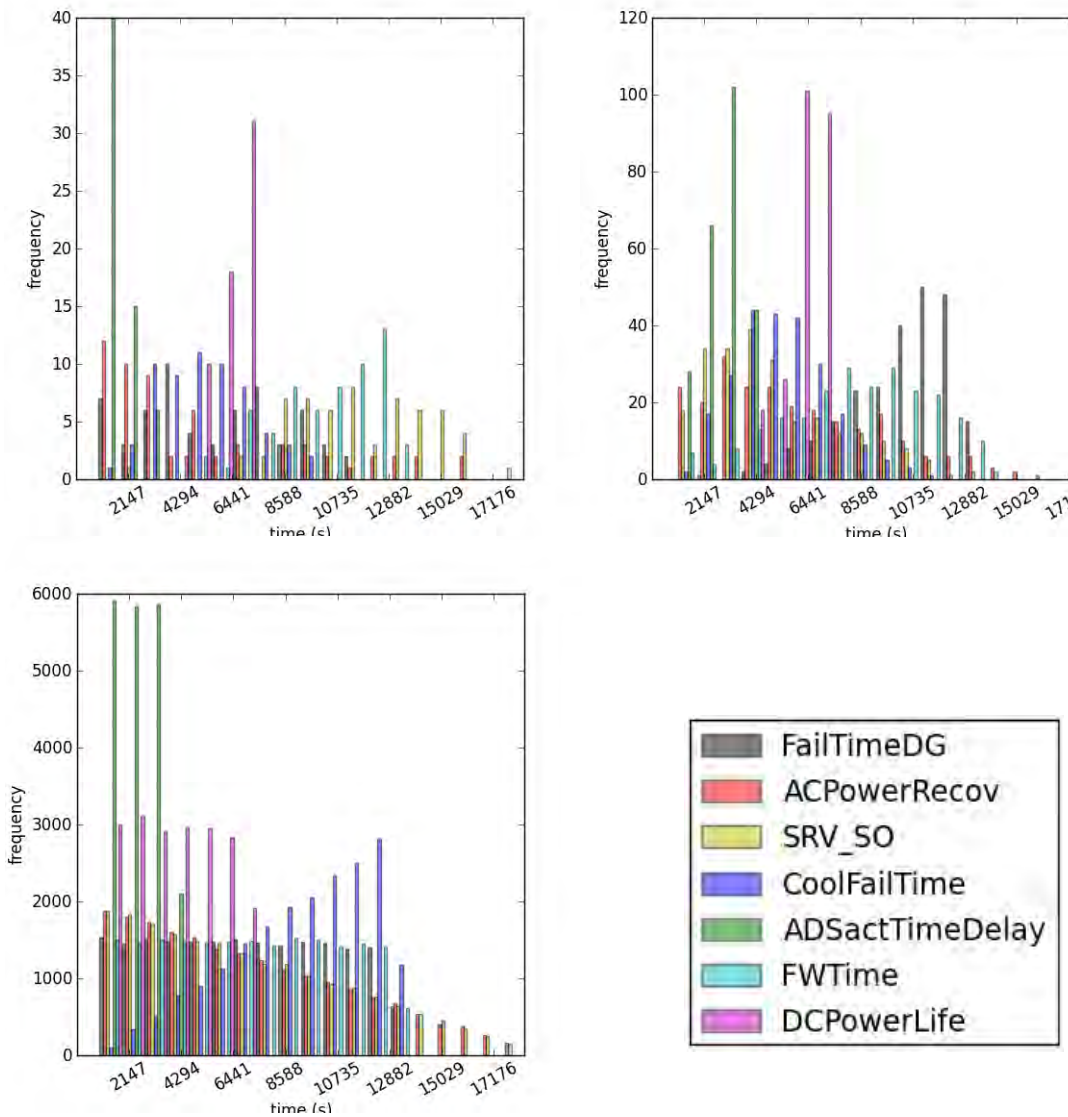

Figure 7-3 9D-MT-all-3C: distribution of input parameters across different clusters for the blue (top left), green (top right) and red (bottom left)

7.3 Case 9D-MT-successes-3C

In Section 7.2 we were able to draw conclusions about how to reach core damage but not much was possible to be deducted for the success cases. In this respect, we performed a second analysis by considering only data point that lead to system success. This analysis, called 9D-MT-successes-4C, consists of:

- Only data points that lead to success
- Nine dimensions
- Output variable is maximum clad temperature

Using HDViz (see Appendix C) and the 9D-MT-all-3C data-set, we were able to obtain four crystals/clusters as shown in Figure 7-4. Topological structure of Clad max temperature as a 9-dimensional surface was characterized by a single local minima and 3 local maxima as indicated in Table 7-2.

Figure 7-5 show the projection of the three crystal for each dimension including regression curve: the x-axis corresponds to an output variable (maximum clad temperature) while the y-axis corresponds to an input variable. In addition, Figure 7-6 shows, for each crystal, the histogram distribution of a set of timing of events.

From Figure 7-5 and Figure 7-6, and by looking at the regression curve obtained, we can see the following:

- As expected, an early AC power recovery is necessary and sufficient condition to obtain success
- From blue crystal, an earlier FW injection time is also another sufficient condition to obtain a positive simulation outcome *even* for a short battery life.
- From the purple crystal we can see that for an early high-pressure injection (both RCIC and HPCI) failure time and a short battery life (i.e., early ADS activation), AC power needs to be recovered as soon as possible
- By looking at the green crystal regression line, in the event of early high-pressure injection (both RCIC and HPCI) failure time, an early SRV stuck open event and a late FW injection availability time, the system can be kept in a safe state only through early AC power recovery

Table 7-2: Minima and maxima of the crystals of Figure 7-4

Crystal color (see Figure 7-4)	*Min*	*Max*
Red	1008.80	2591.47
Green	1008.80	2444.34
Blue	1008.80	2051.76
Magenta	1008.80	2509.11

Again, this type of data analysis points to possible risk-informed margins management approaches. For example, the FW time is important to success (even in the case where the batteries fail early) – consequently plant procedural or hardware modifications to improve FW performance under SBO conditions could be beneficial.

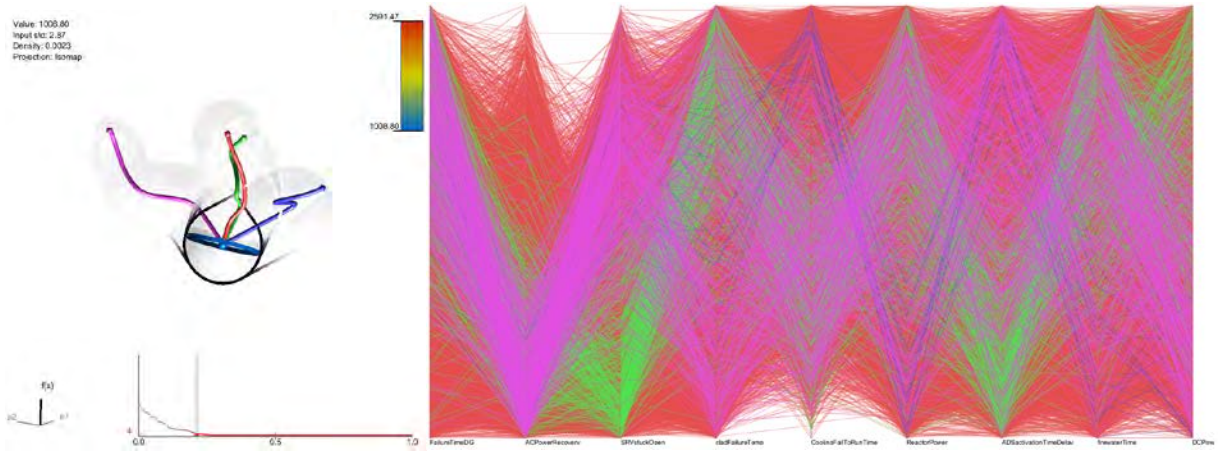

Figure 7-4: 9D-MT-successes-3C: topological summary (left) and parallel coordinate plots for all three clusters (right)

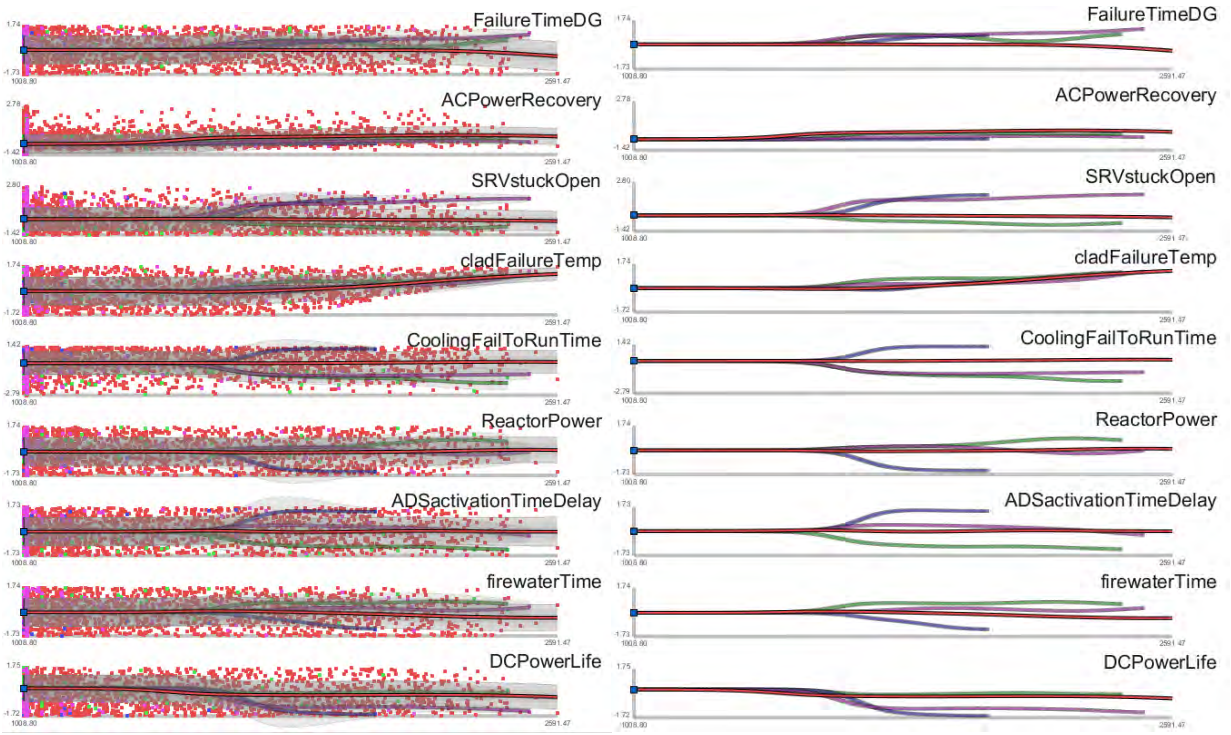

Figure 7-5: 9D-MT-successes-4C: inverse coordinate plots with (left) and without (right) points projection

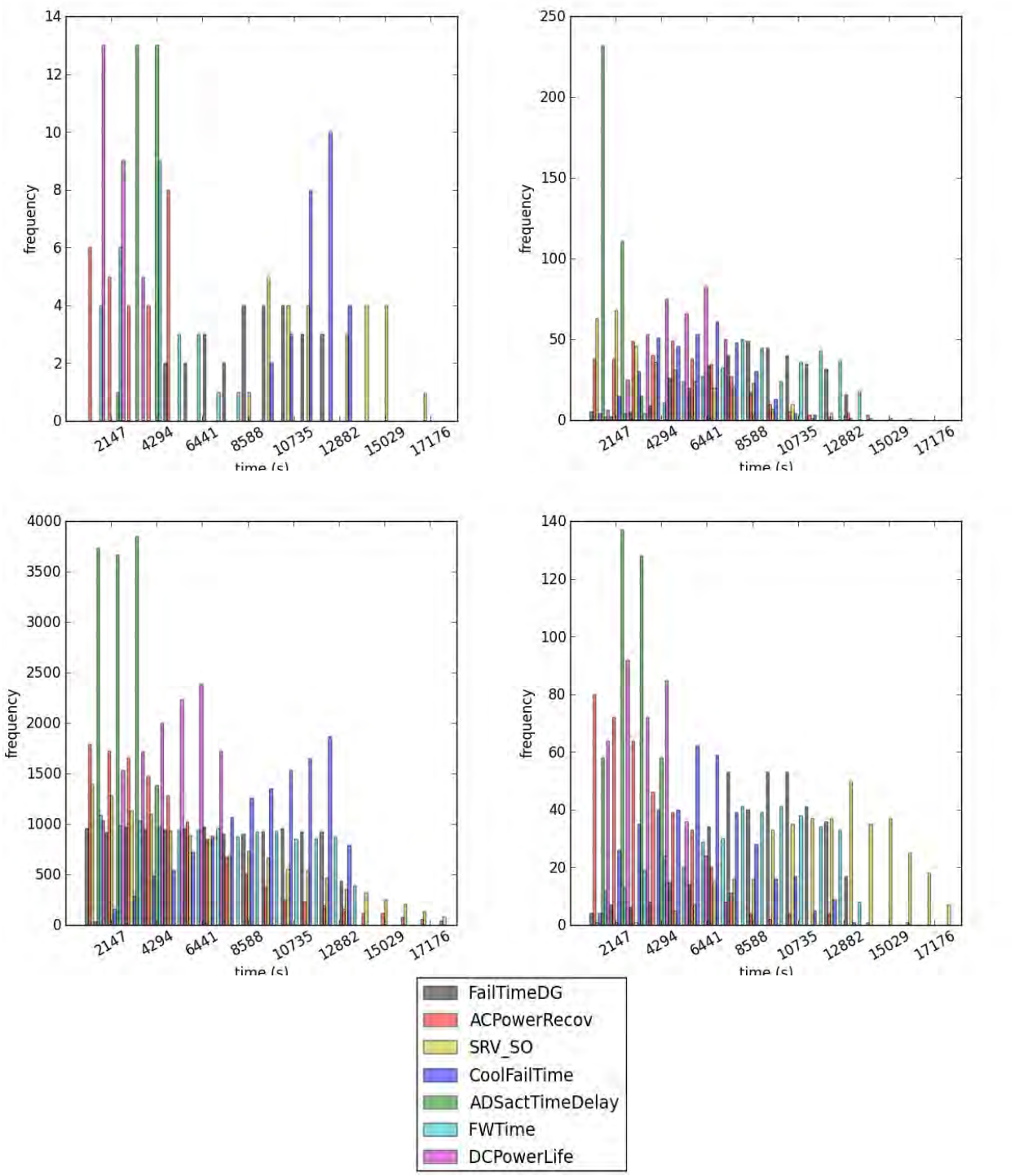

Figure 7-6: 9D-MT-successes-4C: distribution of input parameters across different clusters for the blue (top left), green (top right), red (bottom left) and magenta (bottom right)

8. COMPARISON WITH STATIC PRA RESULTS

In this section we compare some of the results of the RISMC analysis obtained in Sections 6 and 7 with the ones obtained from the "static analysis" (event tree based) of the BWR LOOP+SBO scenario.

The results obtained in Sections 6 and 7 highlighted how much information can be gathered by fully considering system dynamics coupled with appropriate statistical models. This could be extended if more advanced statistical models such as Markov, queuing, or network models were employed.

As an example, the fact that in a scenario AC power recovery has been sampled to occur at a certain time instant does not guarantee that simulation outcome will necessarily be success. By determining the limit surface it is possible to measure the specific timing of AC power recovery (for example) that cause the simulation outcome to transition from failure to success. Such information can be used to effectively inform reactor operators on how much time is needed to recover AC power in a SBO event and effectively prioritize tasks during a SBO accident.

As a summary, from the analysis of Sections 6 and 7 we were able to:

- Perform a quantitative evaluation of the effects of power uprate on BWR LOOP+SBO accident scenario. In particular, we have identified the safety parameters that were more relevant in the analysis such as T_{ADS}, T_{FW} and T_{CD} and we measured the consequence of the increased reactor power on them

- Quantify the importance on DGs failure time, high pressure injection failure time (both RCIC and HPCI), FW availability and STV stuck open event and AC power recovery (either DGs or off-site power grid)

By looking at the results presented in Sections 6 and 7 and the PRA model structure of Section 4 we identified the following qualitative observations:

- The PRA model were not able to quantify effects of power uprate on the safety parameters of system considered. Parameters such as "core power level" are not typically included in static PRA models since they include just the probabilistic elements related to accident scenarios.

- The provided PRA model included a path leading to containment venting action. In the RELAP-5 model such events were never queried since core damage condition was reached before the conditions requiring containment venting were met. Note that if we had investigated other accident scenarios or initiating events, containment venting conditions may have been met.

- Importance of the actions to extended ECCS operation was lower in the "Dynamic Analysis" due to the fact that ADS activation (when PSP HCTL are reached) often occurred before then end of the actual battery life and thus, i.e., no extended ECCS operation were required

- AC recovery time (through DGs or off-site power grid), failure of high-pressure injection (both RCIC and HPCI) and FW availability were the three most important parameters for both the static and dynamic analysis

- Failure time of DGs was a major player in both the dynamic and static analysis.

In more detail we want to highlight the following:

- The BWR LOOP+SBO PRA model provided a source of information in the early phase of the analysis in order to identify set of stochastic parameters that would be relevant in the analysis

- The RISMC analysis, as a contrast to the "static analysis" of the PRA models, highlights how dynamic analysis aims to complement the static analysis by adding more quantitative information and represents the actual physics of either success or failure scenarios that can help decision makers to performed risk-informed decisions.

9. SUMMARY

9.1 Analysis considerations

In this report we wanted to demonstrate the capabilities of the RISMC methodology in order to assess the impact of core power uprate on a BWR SBO accident scenario using state-of-the-art tools and machine-learning based algorithms.

In summary we performed the following:

- Built a T-H BWR model and we implemented using RELAP-5
- Used an existing T-H BWR model for RELAP-7 used for SBO calculations
- Implemented a statistical model for a SBO accident scenario
- Identified and quantified how the safety relevant parameters for a SBO accident scenario change when reactor power is increased above its nominal value; in addition we evaluated how adaptive sampling algorithms can drastically decrease the computational time of such
- Identified limitation of state-of-practice tools that model accident scenarios in a static fashion and without fully considering system dynamics and timing/sequencing of events
- Performed an uncertainty analysis on a set of parameters characteristic of the BWR model using advanced analysis and visualization tools

The set of analysis performed gave both a broad and detailed investigation on how a reactor power uprate affects plant operational outcomes such as the time available to reactor operators and staff to perform recovery procedures to:

1. Maintain RPV pressurized in order to guarantee reactor cooling using high-pressure injection system (RCIC or HPCI)
2. Recover AC power (either DGs or off-site power gird)
3. Align fire-water in order to cool core after depressurization occurs

Ability to maintain RPV pressurized has been proved essential in order to increase the possibility of AC power recovery. For this event, we identified the following parameters as relevant:

- Failure time of DGs
- PSP heat capacity
- High-pressure injection availability (i.e., RCIC and HPCI)
- SRV reliability

Note that battery life, for the system considered, is not included in the list presented above. This is for the following reasons:

- We assumed a high reliability values for DC systems, i.e. batteries
- The ability to maintain RPV pressurized is driven mainly on the PSP HCTL limits; hence importance of battery life is obscured by PSP heat capacity

Note also that a different ADS activation strategy might boost importance of battery life.

Alignment of fire-water operations start after the RPV has been depressurized and hence the following parameters have been found relevant:

- Failure time of DG
- Time that RPV have been kept pressurized

9.2 Potential Model Improvements

The RELAP-5 model that we built had some intrinsic limitations. Due to time constraints we were not able to resolve such limitations. As a model improvement, we have identified the following:

- HPCI/RCIC Early Stability – It was found that sampling HPCI or RCIC to fail before ten minutes into the simulation caused it to crash. To get around this, the sampling was changed from 0 to 8 hours to 10 minutes to 8 hours. It would improve the model to fix this early stability problem and be able to change the lower limit on the sampling back to the beginning of the simulation.

- Wetwell – the wetwell, as it stands, was built specifically to produce realistic pre-blowdown temperature and pressure results, with little/no consideration for post-blowdown data or how the wetwell would interact with other components pre-blowdown. This was done because attempts at a more complex torus were either unstable or inaccurate, and the pre-blowdown pressure and temperature were deemed the most important pieces of data for the current scope of the project. The wetwell modeling could be improved with a more complex wetwell component that more accurately models the thermal stratification in the wetwell, allowing for more realistic interaction between the wetwell and drywell in general and between the wetwell and RPV after depressurization.

- Drywell – the model for the Drywell is very basic and needs to be reworked with more complexity. The drywell can be improved with a more detailed approach that attempts to more accurately reflect where pump seal LOCA scenarios would be venting steam, and more accurately reflect where the connection between the wetwell and drywell inserts into the wetwell. This would bring greater realism to the Drywell and Wetwell simulation, allowing for a greater variety of transients to be examined.

- Connection between the Drywell and Wetwell – In reality, the connection between the Drywell and Wetwell is a complex piece of piping, whereas in the model used it is a simple one volume component that greatly oversimplifies the connection, damaging the realism of the interaction between the Drywell and Wetwell. This can be corrected with a more

complex approach to this connection, adding realism to the interaction between the Drywell and Wetwell and allowing for more realism in the Pump Seal LOCA model.

- Seal LOCA and Detailed Seal Failure Model – Attempts to model a Pump Seal LOCA were less successful than desired – in particular, low GPM leaks caused RELAP5-3D to become extremely unstable, crashing over half of the simulations attempted. It is believed that many of the problems with the Pump Seal LOCA will be fixed by improving the Drywell and Wetwell models. Additionally, the model for when and how the Pump Seal LOCA occurred can be improved, as it is currently a simple time based event, rather than being evaluated on the basis of the pump heating up and heat induced seal failure. Improving this will bring greater realism to Pump Seal LOCA simulations.

- ADS Strategies – The ADS strategy employed in the current simulation is to simply open all SRVs fully and leave them open. An alternate strategy to be explored is to cycle the SRVs on and off to provide a slower, more controlled blowdown, potentially with less risk for briefly uncovering the core in the blowdown process. The rapid depressurization never caused risk to the cladding integrity in our simulations, but venting a great deal of the RPV contents quickly has the potential to expose the core, thus alternate strategies are worth examining. Doing as such gives more parameters to evaluate, as it is never guaranteed that the operators will follow the alternate blowdown procedure perfectly, and allows for more variety and detail in how transients evolve.

- AC Powered Conditions – Due to instabilities caused by the jetmixer of the core Recirculation Line, it was removed. Because the jetmixer used momentum induced flow to produce the desired effects, for SBO conditions it is not vital to have it in the simulation, as there is not enough flow through the jetmixer to significantly affect the state of the plant. The downside of this is that the model can no longer accurately simulate steady state plant conditions, so we have to end the transient at AC power recovery instead of running it all the way to some safety condition that better guarantees we have recovered the safety integrity of the plant. Being able to model AC Powered Conditions brings greater accuracy and realism to the model, particularly for scenarios where we have AC power for an extended period of time, or recover power after a period of Station Blackout, allowing for more extensive PRA capabilities.

- Secondary Side – the model currently uses a boundary conditions to represent the Main Steam Turbine and Bypass, and it would expand our simulation capabilities to more fully simulate the Steam side of the plant and to actually model components like the turbine and condenser. This is a lower priority project than some of the others mentioned here, as it would provide less return for the work invested, but would still give more failure modes to be examined and parameterized for Monte Carlo sampling and is a possible expansion of the model.

9.3 Analysis improvements

From an analysis point of view we have identified possible improvements:

- Level 2 Analysis – the most ambitious goal to increase the analysis scope would be to expand the scope of the simulation to a Level 2 Analysis using tools like SCDAP or MELCOR. SCDAP is a module to expand the capabilities of RELAP5-3D, normally a Level 1 code, to be able to do Level 2 Analyses, and MELCOR is a separate code entirely built to do Level 2 Analyses. This would allow the model to continue after core damage

has begun, and to examine the extent of the core damage and potential for release to the environment, adding a great deal of detail and realism to the model and expanding the scope of any PRA work done using RAVEN and the model.

- Economic evaluation – Despite the fact a successful FW injection would guarantee system success we acknowledge the fact that it would create an economical loss for the plant owner/operator. Thus we believe it would beneficial to identify the economic impact of each scenario other than considering only the final outcome of the simulation, i.e., success or failure.

- Material aging – The objective of the RISMC project is to identify the impact of material aging and power uprate on system performance and limitations. In this report we focused primarily on power uprate while material ageing has been considered only on the failure pressure of the containment (which was not influential since containment failure condition was never reached). Thus, it would appropriate to include material ageing by adding statistical models in the analysis for the components subject to ageing.

- Quantitative comparison with static PRA – In this report, we only compared the differences between the static PRA and the RISMC methodology in a qualitative fashion. In future analyses, it will be possible to numerically compare the two approaches in order to quantify differences (and similarities) directly.

10. REFERENCES

[1] Smith, C., Rabiti, C., & Martineau, R., INL/EXT-11-22977, *Risk Informed Safety Margins Characterization (RISMC) Pathway Technical Program Plan*. Idaho National Laboratory

[2] RELAP5 Code Development Team. (2012). *RELAP5-3D Code Manual*. INL, (2012).

[3] A. Alfonsi, C. Rabiti, D. Mandelli, J. Cogliati, and R. Kinoshita, "Raven as a tool for dynamic probabilistic risk assessment: Software overview," in Proceeding of M&C2013 International Topical Meeting on Mathematics and Computation, CD-ROM, American Nuclear Society, LaGrange Park, IL (2013).

[4] Gertman, D., Blackman, H., Marble, J., Byers, J., and Smith, C., "*The SPAR-H Human Reliability Analysis Method"*, NRC (2005).

[5] Zhang, H. H. Zhao, L. Zou, D. Andrs, J. Peterson, R. Berry, R. Martineau, INL/EXT-13-29887, *RELAP-7 Simulation Resolving an SBO Scenario on a Simplified Geometry of a BWR*, (2013).

[6] Larson, F.R., Miller, J., "A Time-Temperature Relationship for Rupture and Creep Stress," Transactions of the American Society of Mechanical Engineers, p. 765 (1952).

[7] Ruger, C. J. and J. C. Higgins, BNL-NUREG-49115, *Reactor coolant pump seal issues and their applicability to new reactor design*, (1993).

[8] J.J. Cherry, J.A. Smith, H.L. Graves, "NUREG-DC-6706: Capacity of Steel and Concrete Cantinament Vessels with Corrosion Damage", Division of Enginerring Technoclogy, Office of Nuclear Regulatory Research, Washington (2001).

[9] C. J. C. Burges, "A Tutorial on Support Vector Machines for Pattern Recognition," Data Min. Knowl. Discov. vol. 2, no. 2, pp. 121–167 (Jun. 1998).

[10] D. Mandelli and C. Smith, "Adaptive sampling using support vector machines," in Proceeding of American Nuclear Society (ANS), San Diego (CA), vol. 107, pp. 736-738 (2012).

[11] H. Edelsbrunner, D. Letscher, and A. J. Zomorodian. Topological persistence and simplification. Discrete and Computational Geometry, vol. 28, pp.511–533 (2002).

[12] S. Gerber, P.-T. Bremer, V. Pascucci, and R. Whitaker, "Visual exploration of high dimensional scalar functions," IEEE Transactions on Visualization and Computer Graphics, vol. 16, pp.1271–1280 (2010).

[13] D. Maljovec, B. Wang, V. Pascucci, P.-T. Bremer, M. Pernice, D. Mandelli, and R. Nourgaliev, "Exploration of high-dimensional scalar function for nuclear reactor safety analysis and visualization," in Proceeding of M&C2013 International Topical Meeting on Mathematics and Computation, CD-ROM, American Nuclear Society, LaGrange Park, IL (2013).

Appendix A: Limit Surface Evaluation

This section explains how the limit surfaces shown in Sections 6.2 and 6.3 have been evaluated. We employed Support Vector Machine (SVM) based algorithms.

Given a set of *N* multi-dimensional samples $\boldsymbol{x}_i$ and their associated results $y_i = \pm 1$ (e.g., $y_i = +1$ for system success and $y_i = -1$ for system failure), the SVM finds the boundary (i.e., the decision function) that separates the set of points having different y_i. The decision function lies between the support hyper-planes which are required to:

- Pass through at least one sample of each class (called support vectors)
- Not contain samples within them

For the linear case, see Figure A-1, the decision function is chosen such that distance between the support hyper-planes is maximized.

Without going into the mathematical details, the determination of the hyper-planes is performed recursively and updated every time a new sample has been generated. Figure 11-1 shows the SVM decision function and the hyper-planes for a set of points in a 2-dimensional space having two different outcomes: $y_i = +1$ (green) and $y_i = -1$ (red).

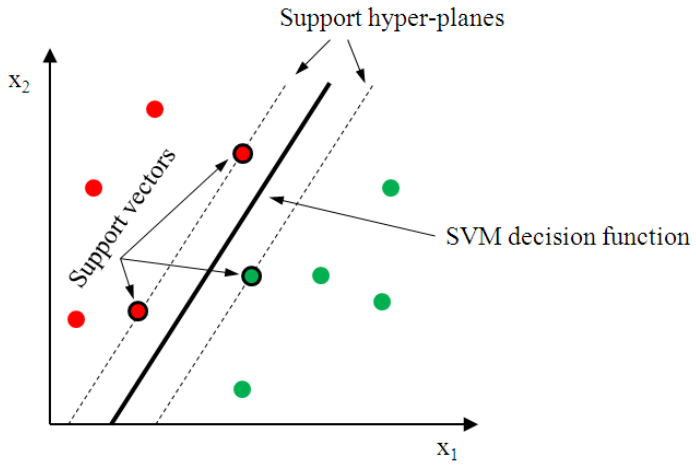

Figure A-1: Limit surface evaluation using SVMs

The transition from a linear to a generic non-linear hyper-plane is performed using the kernel trick. This process involves the projection of the original samples into a higher dimensional space known as featured space generated by kernel functions $K(\boldsymbol{x_i}, \boldsymbol{x_j})$:

$$K(\boldsymbol{x_i}, \boldsymbol{x_j}) = \exp\left(-\frac{\|\boldsymbol{x_i} - \boldsymbol{x_j}\|}{2\sigma^2}\right)$$

Appendix B: Preliminary Evaluation of Adaptive Sampling Algorithms

As shown in Section 6, nuclear simulations are often computationally expensive, time-consuming, and high-dimensional with respect to the number of input parameters. Thus exploring the space of all possible simulation outcomes is infeasible using finite computing resources. This is a typical context for performing adaptive sampling where a few observations are obtained from the simulation, a surrogate model is built in order predict behavior of the system (e.g., maximum core temperature), and new samples are selected based on the model constructed (see Figure B-1).

The surrogate model is then updated based on the simulation results of the sampled points. In this way, we attempt to gain the most information possible with a small number of carefully selected sampled points, limiting the number of expensive trials needed to understand features of the simulation space. From a safety point of view, we are interested in identifying the limit surface, i.e., the boundaries in the simulation space between system failure and system success. The generic structure of an adaptive sampling algorithm is shown in Figure B-2.

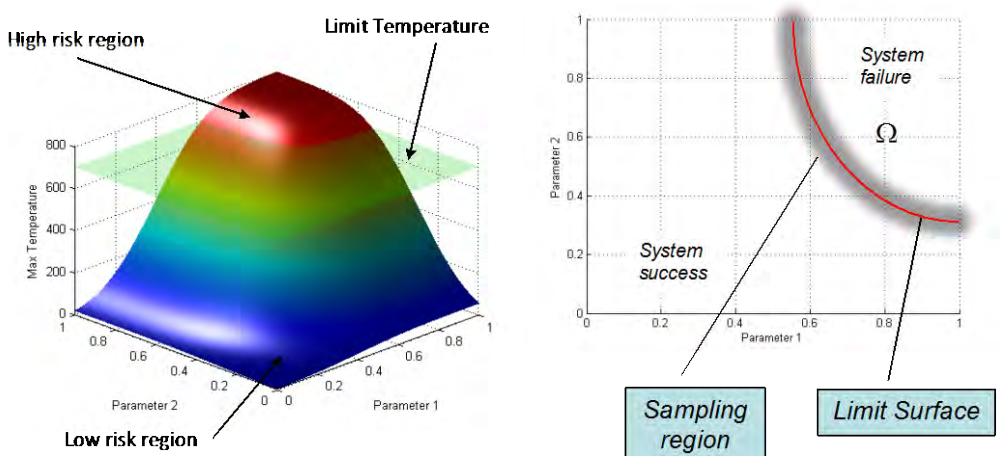

Figure B-1: Max core temperature as function of 2 parameters and limit/fail temperature (left) and plot of their intersection: limit surface (right)

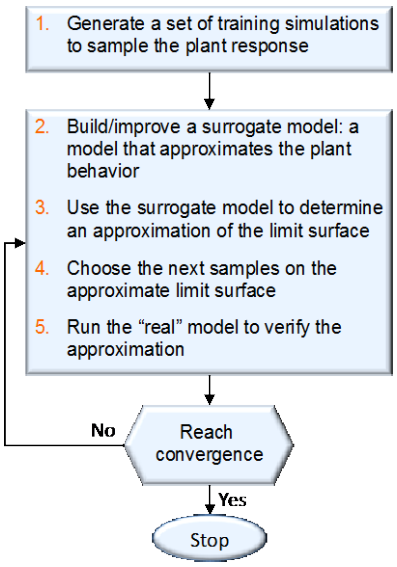

Figure B-2: Generic scheme for adaptive sampling algorithms

Figure B-3 shows an example of limit surface determination for a simplified PWR system during a station blackout (SBO) scenario. Two stochastic variables are considered: initial time after scram (*x* axis) and duration (*y* axis) of SBO condition. Note how the uncertainty (green and blue lines) associated with the limit surface (black line) after 10 samples (Figure B-3 left) is very wide while after only 60 samples (Figure B-3 right) the limit surface has been completely characterized. Note that the limit surface could have been obtained using Monte-Carlo or Latin Hypercube sampling with a much higher number of samples (about 300 samples). Such improvements can be even higher when a large number of stochastic parameters are considered.

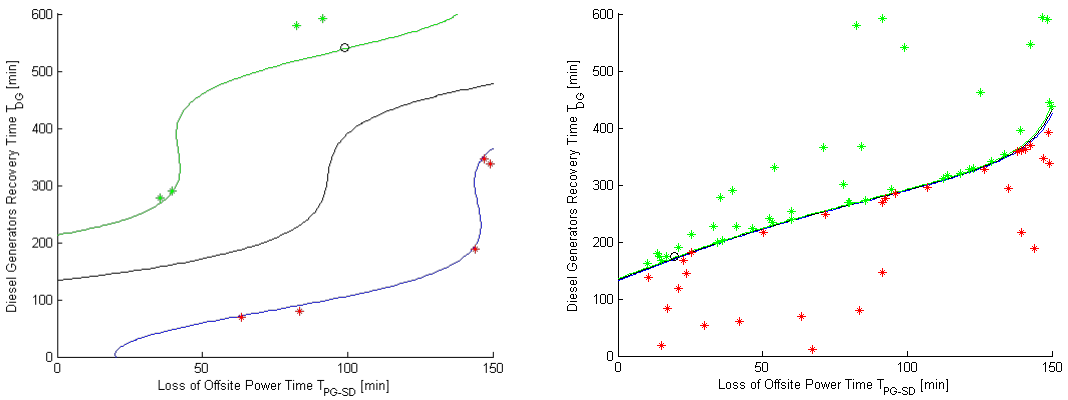

Figure B-3: Limit surface obtained for a simplified PWR system for a SBO scenario after 10 (top) and 60 (bottom) samples

In this report we have implemented a graph-based adaptive sampling scheme. This algorithm begins by directly building a neighborhood structure as the surrogate model (e.g. a relaxed Gabriel graph) on the initial training data. It then creates a candidate set by first obtaining linearly interpolated points along spanning edges of the graph, and introducing a random perturbation along all dimensions to these points.

The candidate set we obtained is arguably sparser, however introducing a certain amount of perturbation to the linearly interpolated points enables us to explore the region surrounding the limit surface further. Note that this algorithm does not employ any mathematical model (e.g., Gaussian Process Model) to infer the location of the limit surface but only relies on the data point location. The graph obtained during each round changes only slightly, such that without a random perturbation the candidate points are generally located linearly along the edge of the graph, which is less desirable.

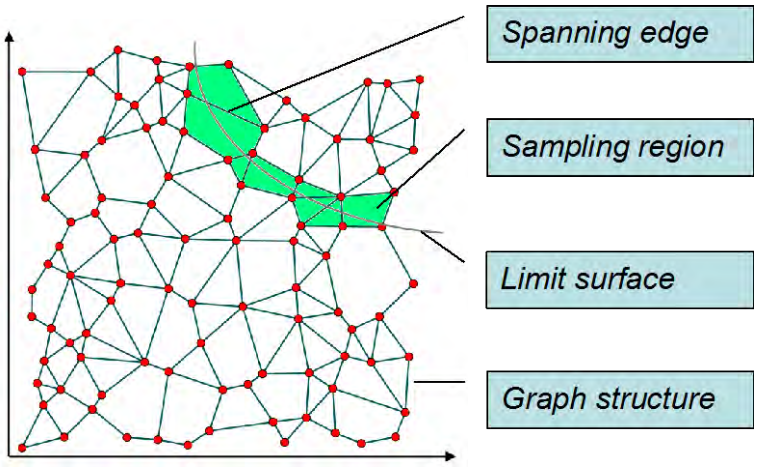

Figure B-4: Scheme of Graph base adaptive sampling algorithm

We performed a set of preliminary tests to evaluate the performance of adaptive sampling schemes. In particular, in this report we focused on the evaluation of the limit surfaces presented in Sections 6.2 and 6.3. The results shown in Table 11-1 indicate a great reduction in terms of simulation runs needed in order to identify such limit surfaces.

Table B-1: Preliminary adaptive sampling results

Test case	*Monte-Carlo samples*	*Adaptive sampling samples*	*Reduction*
*(*Section 6.2*)*	700	~ 60	91.5 %
(Section 6.3)	800	~ 60	92.5 %

Appendix C: High–dimensional data analysis tools

The need for software tools able to both analyze and visualize large amount of data generated by Dynamic PRA methodologies has been emerging only in recent years. In the past 2 years, INL and University of Utah have developed a software tool able to analyze multi-dimensional data: HDViz.

HDViz model the relations between output variables (e.g., maximum clad temperature) and stochastic/uncertain parameters as high-dimensional functions. In this respect, HDViz segments the domain of these high-dimension functions into regions of uniform gradient flow by decomposing the data based on its approximate Morse-Smale complex (see Figure C-1). Points (i.e., simulation runs) belonging to a particular segmentation have similar geometric and topological properties, and from these it is possible to create compact statistical summaries of each segmentation. Such summaries are then presented to the user in an intuitive manner that highlights features of the dataset which are otherwise hidden (see Figures C-2 and C-3). In addition, the visual interfaces provided by the system are highly interactive and tightly integrated, providing users with the ability to explore various aspects of the datasets for both analysis and visualization purposes.

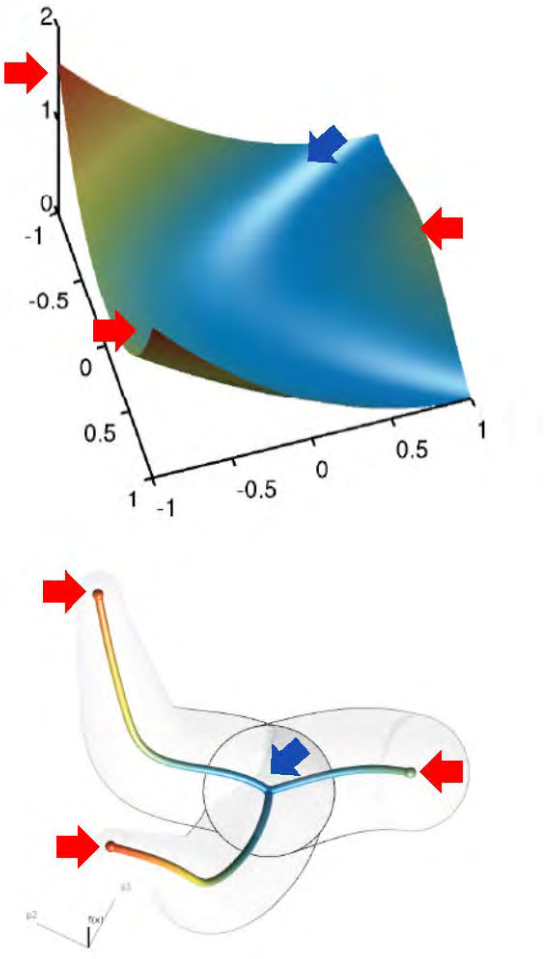

Figure C-1: Representation example of a 3-dimensional function in terms of crystals that connect local minima to local maxima. In this case a single minima (blue arrow) and 3 maxima (red arrows) have been

identified. Three crystal have also been determined; each one shown the path that connect a local minima to a local maxima

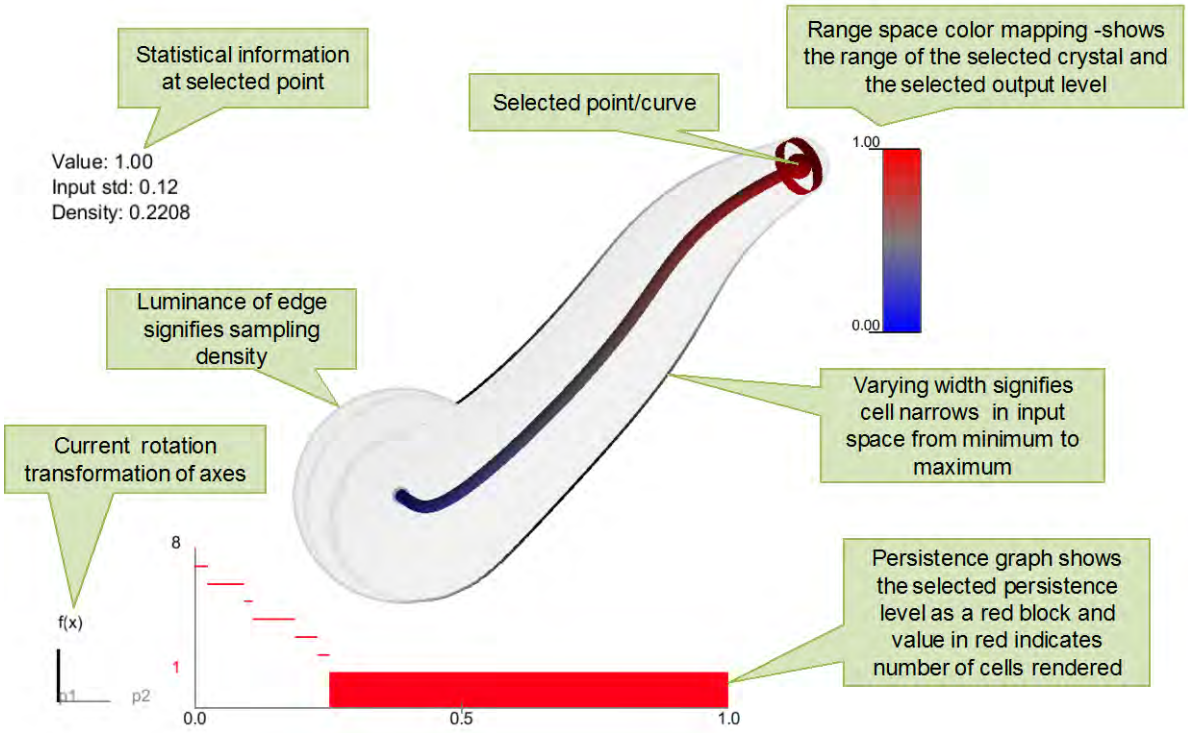

Figure C-2: Summary representation of each crystal

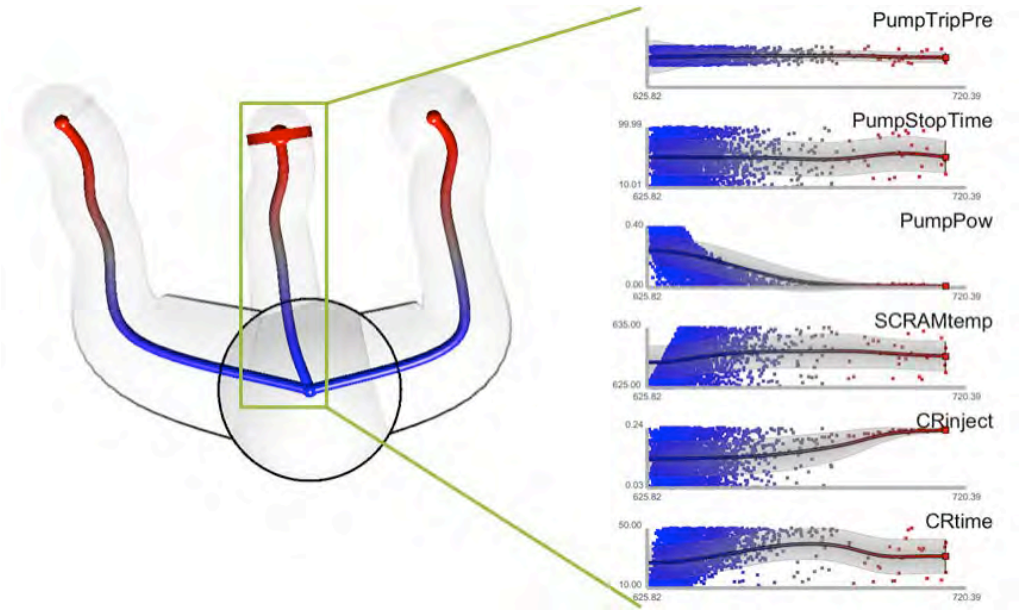

Figure C-3: Statistical information that can be obtained from each crystal for a 6-dimensional case. For each crystal, all the points belonging to it are represented on the right for each of the 6 variables. Regression curves are then inferred